

# Impact of changes in climate and CO<sub>2</sub> on the carbon-sequestration storage potential of vegetation under limited water availability using SEIB-DGVM version 3.02

Shanlin Tong<sup>1,2,3</sup>, Weiguang Wang<sup>2,3\*</sup>, Jie Chen<sup>1\*</sup>, Chong-Yu Xu<sup>4</sup>, Hisashi Sato<sup>5</sup>, Guoqing Wang<sup>6</sup>

<sup>1</sup>State Key Laboratory of Water Resources and Hydropower Engineering Science, Wuhan University, Wuhan, 430072, Peoples R China

<sup>2</sup>State Key Laboratory of Hydrology-Water Resources and Hydraulic Engineering, Hohai University, Nanjing, 210098, Peoples R China

<sup>3</sup>College of Hydrology and Water Resources, Hohai University, Nanjing, 210098, Peoples R China

<sup>4</sup>Department of Geosciences, University of Oslo, Oslo, N-0316, Norway

<sup>5</sup>Japan Agency for Marine-Earth Science and Technology, Yokohama, 236-0001, Japan

<sup>6</sup>Nanjing Hydraulic Research Institute, Nanjing, 210029, Peoples R China

\*Correspondence to: Weiguang Wang ([wangweiguang2016@126.com](mailto:wangweiguang2016@126.com)); Jie Chen ([jiechen@whu.edu.cn](mailto:jiechen@whu.edu.cn))

## Abstract

Documenting year-to-year variations in carbon-sequestration storage potential in terrestrial ecosystems is crucial for the determination of carbon dioxide (CO<sub>2</sub>) emissions. However, the magnitude, pattern and inner biomass partitioning of carbon-sequestration storage potential, and the effect of the changes in climate and CO<sub>2</sub> on inner carbon stocks, remain poorly quantified. Herein, we use a spatially explicit individual based-dynamic global vegetation model to investigate the influences of the changes in climate and CO<sub>2</sub> on the enhanced carbon-sequestration storage potential of vegetation. The modelling included a series of factorial simulations using the CRU dataset from 1916 to 2015. The results show that CO<sub>2</sub> predominantly leads to a persistent and widespread increase in above-groundlight-gathering vegetation biomass carbon-stocks (AVBCGVBC) and below-groundwater-gathering vegetation biomass carbon-stocks (BVBCWVBC). Climate change appears to play a secondary role in carbon-sequestration storage potential. Importantly, with the mitigation-intensification of water stress, the magnitude of the above-light- and below-groundwater-gathering responses in vegetation carbon-stocks gradually decreases/increases. Plants adjust carbon allocation to decrease the ratio between GVBC and WVBC for capturing more water, and the ratio between AVBC and BVBC increases to capture CO<sub>2</sub> and sunlight. Changes in the pattern of vegetation carbon storage was linked to regional-zonal limitations in water,

32 which directly weakens and indirectly regulates the response of potential vegetation carbon stocks to a  
33 changing environment. Our findings differ from previous modelling evaluations of vegetation that  
34 ignored inner carbon dynamics and demonstrates that the long-term trend in increased vegetation  
35 biomass carbon stocks is driven by CO<sub>2</sub> fertilization and temperature effects that are controlled by water  
36 limitations.

## 37 **1 Introduction**

38 As a result of the changes in climate and atmospheric carbon dioxide (CO<sub>2</sub>), the terrestrial ecosystem  
39 carbon cycle exhibits remarkable trends in interannual variations, which induce uncertainty in estimated  
40 carbon budgets (Erb et al., 2018; Keenan et al., 2017). Recent studies assessing interannual fluctuations  
41 in terrestrial carbon sinks have shown that the land carbon cycle is the most uncertain component of the  
42 global carbon budget (Ahlstrom et al., 2015; Piao et al., 2020; Jung et al., 2017; Humphrey et al., 2018;  
43 Gentine et al., 2019; Humphrey et al., 2021). These uncertainties result from an incomplete understanding  
44 of vegetation biomass carbon production, allocation, storage, loss, and turnover time (Bloom et al., 2016).  
45 The extent and distribution of vegetation carbon storage is central to our understanding of how to  
46 maintain a balanced land carbon cycle. Changes in terrestrial vegetation carbon storage have a significant  
47 effect on atmospheric CO<sub>2</sub> concentrations and determine whether biomes become a source or sink of  
48 carbon (Erb et al., 2018; Humphrey et al., 2018; Terrer et al., 2021). Therefore, investigating the  
49 processes producing changes in carbon storage is key to improving the accuracy of estimated terrestrial  
50 carbon budgets, and to tap the greenhouse-gas moderation potentials of vegetation (Ipcc, 2007; Roy et  
51 al., 2001).

52

53 The atmospheric CO<sub>2</sub> concentration are affected by the vegetation carbon stock, while the long-term  
54 trend of vegetation carbon storage capacity is also affected by the changes in climate and CO<sub>2</sub>. The  
55 response of vegetation carbon storage to greenhouse effects results from two mechanisms, direct effects  
56 of CO<sub>2</sub> on photosynthesis and indirect effects of changes in climate change and CO<sub>2</sub> on photosynthesis,  
57 respiration, and sequestration (Schimel et al., 2015; Gentine et al., 2019; Cheng et al., 2017). Since the  
58 beginning of industrialization, there has been a noticeable enhancement in the capacity of storing and  
59 sequestering carbon, which is needed for stabilizing greenhouse gas concentrations and mitigating global

60 warming (Chen et al., 2019; Pan et al., 2011; Le Noë et al., 2020; Magerl et al., 2019; Bayer et al., 2015;  
61 Harper et al., 2018). Due to the interaction between terrestrial vegetation and a changing environment,  
62 both photosynthesis and respiration of the vegetation also changed. To better absorb CO<sub>2</sub> and sunlight  
63 required for photosynthesis, vegetated zones are gradually covered by vegetation with higher plant height  
64 and wider leaf area. This ~~increase-change~~ has coincided with a widespread change in other vegetation  
65 features, including a positive increase in annual gross primary productivity and a greening of the  
66 biosphere (Madani et al., 2020; Zhu et al., 2016). The spatiotemporal distribution and environmental  
67 drivers in total carbon-sequestration storage potential have been well documented on the basis of model  
68 estimates and satellite-based assessments (Erb et al., 2007; Erb et al., 2018; Bazilevich et al., 1971;  
69 Saugier et al., 2001; Bartholome and Belward, 2005; Olson et al., 1983; Pan et al., 2013; Ajtay et al.,  
70 1979; Ruesch and Gibbs, 2008; Kaplan et al., 2011; Shevliakova et al., 2009; Prentice et al., 2011; West  
71 et al., 2010; Hurtt et al., 2011). In contrast, the variability of inner componentsabove and below ground  
72 partitioning of carbon -sequestrationstorage potential has not been extensively studied. Without an  
73 accurate assessment of the dynamics of each fraction, attribution of carbon -sequestration storage  
74 potential to environmental drivers is highly uncertain. Consequently, partitioning potential vegetation  
75 carbon storage and revealing its inner processes are essential to accurately comprehend the current state  
76 of carbon storagesequstration capacity and reveal predict how it will change in the future, both of which  
77 are key instruments in revealing the influence of various drivers on the enhancement-long-term trend of  
78 carbon -sequestrationstorage potential.

79

80 The change of carbon storages in vegetation inner components is not only affected by environmental  
81 factors, but also controlled by allocation scheme of assimilated carbon. Fractional dynamics of the carbon  
82 stock are widely used as a key indicator to investigate the responses of vegetation to environmental  
83 drivers, which also reflect the response strategies of vegetation in environments with different water  
84 limitations (Yang et al., 2010). The variability in vegetation carbon flux is also linked to terrestrial water  
85 availability (Gentine et al., 2019; Seo and Kim, 2019). In arid region, vegetation utilizes a tolerance  
86 strategy to allocate biomass, storing more biomass carbon in roots to resist enhanced water stress (Chen  
87 et al., 2013). Conforming to the optimal partitioning hypothesis, plants store more carbon in shoots and  
88 leaves in environments where water is more available and shift more carbon to roots when water is more

89 ~~limited (Yang et al., 2010; McConnaughay and Coleman, 1999). Thus, potential water limitations impart~~  
90 ~~another constraint on the global ecosystem carbon cycle. Typically, increasing water stress limits the~~  
91 ~~response magnitude of carbon uptake rates through a down regulation of stomatal conductance~~  
92 ~~(Humphrey et al., 2021).~~ Water availability controls both carbon allocation and storage and can  
93 potentially transform ~~regions-zones~~ characterized by a ~~negative-positive~~ response to changes in climate  
94 and CO<sub>2</sub> to ~~regions-zones~~ exhibiting a ~~positive-negative~~ response. For example, global warming  
95 stimulates plant productively. Madani et al. (2020) found that there is a dramatically downward trend in  
96 the tropical productivity. With increased warming, water limitations are predictable to increasingly  
97 reduce the proportion of leaves' biomass, and decrease plant photosynthesis (Ma et al., 2021)warming  
98 has a negative effect on the percentage of roots in dry regions and increases the ratio of above- versus  
99 belowground biomass in wet regions (Ma et al., 2021). This is particularly apparent in tropical regions,  
100 where variations in water availability can result in different responses in the processes involved in the  
101 carbon cycle (Liu et al., 2017). Water limitations have a strong regulating effect on the spatial pattern of  
102 change in vegetation carbon storage, demonstrating the effects of the changes in climate and CO<sub>2</sub> on the  
103 dynamics of the plant organs are affected by the terrestrial water gradient. The differences in the response  
104 mechanisms influencing the vegetation carbon flux among different hydrological regions is related to  
105 plant oversensitivity to hydrological gradients. Thus, it is important to systematically investigate the  
106 distinct responses of carbon sequestrationstorage potential to changes in climate and CO<sub>2</sub> under differing  
107 conditions of water stress.

108

109 As documented above, many studies have investigated the ~~integral-total~~ changes in ~~regionalzonal~~ and  
110 global terrestrial storage of carbon, while few studies have examined trends in the components  
111 partitioning of vegetation carbon storage. ~~by vegetation biomass~~. Large gaps in our knowledge of the  
112 effects of various drivers on the partitioning of carbon stocks in vegetation biomass remain. Meanwhile,  
113 plants adjust carbon allocation scheme to adapt to environmental change. With increased warming,  
114 Importantly, a n increase in the magnitude of water stress may dramatically change or even reverse the  
115 impact of these drivers on ~~above- versus below-groundinner~~ componentspartitioning of carbon   
116 sequestrationstorage potential (Ma et al., 2021). Evaluating the response pattern of carbon stocks to  
117 various drivers under conditions of limited water is elemental for clearly documenting the response

118 mechanism of vegetation carbon ~~sequestration~~ storage potential.

119

120 Here, we use a spatially explicit individual-based dynamic global vegetation model (SEIB-DGVM),  
121 along with the ~~components partitioning method~~ root shoot ratio method (R/S) to (1) systematically  
122 determine the long-term variability of carbon ~~sequestration~~ storage potential and understand its response  
123 mechanisms, and (2) estimate trends in partitioning of potential biomass carbon ~~stocks~~ of vegetation  
124 biomass. Throughout this study, the potential biomass carbon ~~stock~~ biomass carbon stored in vegetation  
125 without anthropogenic disturbance, is recognized as a proxy for the potential of carbon ~~sequestration~~  
126 storage by natural vegetation. ~~Using~~ a set of factorial simulations to isolate responses to environmental  
127 change, we analyse the contributions of multiple driving factors to the trends of two fractions of carbon  
128 ~~stocks~~ at large scales individually. We then conceptualize the role of water availability through an aridity  
129 index (AI), in which hydrological ~~region~~ zones are subdivided by their degree of aridity. By comparing  
130 the differences in the magnitude of response between the fractions of ~~above-light-~~ and water-  
131 gathering ~~belowground~~ carbon ~~stocks~~ for varying degrees of water availability, we assess the effect of  
132 water limitations on the response pattern of potential carbon ~~stocks~~ to changes in climate and CO<sub>2</sub>.

## 133 **2 Model description, experimental design, observational data, and evaluation metrics**

134 In this section, we provided a list of data source (Sect. 2.1), an overview of the modelling concept (Sect.  
135 2.2), the representation of biomass ~~carbon stock~~ carbon stock partitioning in the SEIB-DGVM (Sect. 2.3),  
136 an overview of the experimental scheme used in the model simulations (Sect. 2.4), and ~~the validation of~~  
137 model results an overview about data source and pre-processing of observation dataset for model  
138 evaluation (Sect. 2.5).

### 139 **2.1 Forcing Data**

140 Long-term daily meteorological time-series data are required to run model simulations, including  
141 precipitation, daily range of air temperature, mean daily air temperature, downward shortwave radiation  
142 at midday, downward longwave radiation at midday, wind velocity and relative humidity. These data  
143 were obtained from the Climatic Research Unit (CRU) time series 4.00 gridded dataset (degree 0.5°) for  
144 the period 1901–2015 (Harris et al., 2020). Because the CRU dataset is a monthly based dataset, the

145 monthly meteorological data were converted into daily climatic variables by supplementing daily  
146 climatic variability within each month using the National Centre for Environmental Prediction (NCEP)  
147 daily climate dataset. The NCEP data, displayed using the T62 Gaussian grid with  $192 \times 94$  points, was  
148 interpolated into a  $0.5^\circ$  grid (which corresponds to the CRU dataset) using a linearly interpolation method.  
149 By combining the CRU data, with the interpolated NCEP dataset, we were able to directly obtain the  
150 most of driving meteorological data (details in Sato et al. (2020)). Neither the CRU nor NCEP datasets  
151 included downward shortwave and longwave radiation at midday. Thus, daily cloudiness values in the  
152 NCEP were used to calculate radiation values using empirical functions (Sato et al., 2007).—These data  
153 were all aggregated to a daily timescale with  $0.5^\circ$  resolution to run SEIB-DGVM.

154

155 Atmospheric CO<sub>2</sub> concentrations were collected from Sato et al. (2020), which contains reconstructed  
156 CO<sub>2</sub> concentrations between 1901 and 2015. The statistical reconstruction of global atmospheric CO<sub>2</sub>  
157 was used in this analysis. These reconstructions were based on present annual CO<sub>2</sub> concentrations  
158 recorded from the Mauna Loa monitoring station. These data assume atmospheric CO<sub>2</sub> concentration  
159 was 284 ppm in 1750, and statistically interpolates atmospheric CO<sub>2</sub> concentrations to fill the gap from  
160 1750 to 2015.

161

162 The physical parameters of the soil used in the model include soil moisture at the saturation point, field  
163 capacity, matrix potential, wilting point and albedo. These data were obtained from the Global Soil  
164 Wetness Project 2.

## 165 **2.2 Overview of modelling concept in SEIB-DGVM**

166 Model SEIB-DGVM version 3.02 (Sato et al., 2020) was employed in this study. This is a process-based  
167 dynamic global vegetation model driven by meteorological and soil data. It is an explicit and  
168 computationally efficient carbon cycle model designed to simulate transient effects of environmental  
169 change on terrestrial ecosystems and land-atmosphere interactions. It describes three groups of processes:  
170 land-based physical processes (e.g., hydrology, radiation, aridity), plant physiological processes (e.g.,  
171 photosynthesis, respiration, litter), and plant dynamic processes (e.g., establishment, growth, mortality).  
172 Twelve plant functional types (PFTs) were classified. During the simulation, a sample plot was  
173 established at each grid box, and then the growth, competition, and mortality of each the individual PFTs

174 within each plot were modelled by considering the specify conditions for that individual as it relates to  
175 other individuals that surround it (Sato et al., 2007).

176

177 SEIB-DGVM treats the relationships between soil, atmosphere, and terrestrial biomes in a consistent  
178 manner, including the fluxes of energy, water, and carbon. Based on specified climatic conditions and  
179 soil properties, SEIB-DGVM simulates the carbon cycle, energy balance, and hydrological processes.

180 SEIB-DGVM utilizes three computational time steps: (1) During the growth phase, the metabolic  
181 procedures including photosynthesis, respiration, and carbon allocation are executed for each individual  
182 tree every simulation day. (2) The monthly process of tree growth including reproduction, trunk growth,  
183 and expansion of a cross-sectional area of the crown are executed. (3) On the last day of each year, the  
184 height of the lowest branch increases as a result of purging crown disks, or self pruning of branches, at  
185 the bottom of the crown layer. (1) a daily time step for all physical and physiological processes, including  
186 soil decomposition and tree growth, (2) a monthly time step for tree growth, and (3) an annual time step  
187 for tree establishment and death. The simulated unit of the model is a 30 m × 30 m spatially explicit

188 ‘virtual forest’. A grass layer was placed under the woody layer, and provides for a comprehensive,  
189 spatially explicit quantification of terrestrial carbon sinks and sources. The soil depth was set at 2 m and  
190 was divided into 20 layers, each with a thickness of 0.1 m. The photosynthetic rate of a single-leaf was  
191 simulated following a Michaelis-type function (Ryan, 1991). Respiration was divided into two types:  
192 growth respiration and maintenance respiration. Growth respiration is defined as a construction cost for  
193 plant biosynthesis, which is quantified by the chemical composition of each organ (Poorter, 1994).

194 Maintenance respiration of live plants occurs every day regardless of the phenological phase, and is  
195 controlled by the temperature and nitrate content of each organ (Ryan, 1991). For a wide variety of plant  
196 organs, the maintenance respiration rate is linearly related to the nitrogen content of living tissue. The  
197 relative proportions of nitrogen in each organ for any PFT are linearly correlated. N-deposition doesn't  
198 include in SEIB-DGVM. Atmospheric CO<sub>2</sub> was envisioned to be absorbed by photosynthesis of woody

199 PFTs and grass PFTs. This assimilated carbon flux was then allocated into all the plant organs (leaf,  
200 trunk, root, and stock), where maintenance respiration and growth respiration occur. The hydrology  
201 module treats precipitation, canopy interception, transpiration, evaporation, meltwater, and penetration.

202

203 ~~SEIB-DGVM differs from other dynamic global vegetation models in that it is a biogeochemical model~~  
204 ~~that represents plant structure in three dimensions. This representation of vegetation dynamics has two~~  
205 ~~advantages. First, it directly uses *in situ* data about PFT dynamics and structure as tuning or validation~~  
206 ~~data, without adding additional assumptions. Second, sunlight and other resources are distributed among~~  
207 ~~individuals without human disturbances, leading to a more properly calculated and accurate~~  
208 ~~representation of the responses of potential vegetation biomass to external environmental change.~~  
209 ~~Therefore, SEIB-DGVM, in general, effectively represents plant competition and function dynamics~~  
210 ~~under environmental change (Sato et al., 2007).~~

## 211 **2.3 ~~Carbon stock~~Carbon stock of vegetation biomass partitioning**

### 212 **2.3.1 Parameterization of daily allocation**

213 Flexible allocation schemes about resources and biomass are set up in the framework of the SEIB-DGVM  
214 biogeochemical model. Based on the updated observation data, the allocation schemes of Boreal Needle-  
215 leaved summer-green trees and Tropical Broad-leaved evergreen trees were improved at SEIB-DGVM  
216 V3.02. Allocation schemes of other PFTs are the same as the original version. Atmospheric CO<sub>2</sub> is  
217 assimilated by the photosynthesis of both woody and grass foliage, and then is added into the non-  
218 structural carbon of the plant. This non-structural carbon of photosynthetic production is allocated to all  
219 the plant organs (foliage, trunk, root, and stock), supplying what is needed for the maintenance and  
220 growth of each organ.—When the non-structural carbon is greater than 0 during the growth phase, the  
221 following dynamic carbon allocation is executed for each individual plant at the daily time scale, such  
222 that:

223 (1) When the fine root biomass ( $mass_{root}$ ) of wood or grass does not satisfy minimum requirements for  
224 fulfilling functional balance ( $mass_{leaf}/FR_{ratio}$ ), the mass of non-structural carbon is allocated to the root  
225 biomass to supplement the deficit. Here,  $mass_{leaf}$  is the leaf biomass, and  $FR_{ratio}$  is the ratio of  $mass_{leaf}$  to  
226  $mass_{root}$  satisfying the functional balance.

227 (2) The stock biomass is supplemented until it is equal to leaf biomass. This scheme is active after the  
228 first thirty days of the growing phase.

229 (3) Woody leaf biomass is constrained by three limitations of the maximum leaf biomass, which are  
230 calculated as follows:



$$231 \quad max_1 = (crown_{area} + \pi crown_{diameter} crown_{depth}) \frac{LA_{max}}{SLA} \quad (1)$$

$$232 \quad max_2 = ALM_1 \frac{\pi(dbh_{heartwood}/2 + dbh_{sapwood}/2)^2 - \pi(dbh_{heartwood}/2)^2}{SLA} \quad (2)$$

$$233 \quad max_3 = \frac{mass_{available}}{RG_f} \quad (3)$$

$$234 \quad mass_{leaf} = \min(max_1, max_2, max_3) \quad (4)$$

235 where  $max_1$ ,  $max_2$ , and  $max_3$  are, respectively, maximum leaf biomass for a given crown surface  
 236 area, cross-sectional area of sapwood, and non-structural carbon;  $SLA$  is a constant of PFT's leaf area  
 237 ( $m^2 g^{-1}$ );  $LA_{max}$  is the plant functional type specific maximum leaf area per unit crown surface area  
 238 excluding the bottom softwood maximum leaf area of PFTs per unit biomass ( $m^2 m^{-2}$ ); and  $ALM_1$  represents  
 239 the area of transport tissue per unit biomass, and is a constant (dimensionless). If the  $mass_{leaf}$  is less than  
 240 the minimum ( $max_1, max_2, max_3$ ), the mass of non-structural carbon is allocated into leaf biomass to  
 241 supplement the deficit.

242 When the leaf area index of grass equals the optimal leaf area index, it stops to allocate non-structural  
 243 carbon to grass leaf Grass leaf biomass is supplemented until the leaf area index of grass equals the  
 244 optimal leaf area index, which are is calculated as:

$$245 \quad lai_{opt} = \frac{\ln par_{grass} - \ln \left\{ \frac{p_{sat}}{lue} \left[ \left( 1 - \frac{cost/SLA}{0.09093 \times dlen \times p_{sat}} \right)^{-2} - 1 \right] \right\}}{eK} \quad (5)$$

246 where  $lai_{opt}$  is the optimal leaf area index ( $m^2 m^{-2}$ );  $par_{grass}$  is the grass photosynthetically active  
 247 radiation ( $\mu mol \text{ photon } m^{-2} s^{-1}$ );  $p_{sat}$  is the light-saturated photosynthetic rate ( $\mu CO_2 m^{-2} s^{-1}$ );  $lue$   
 248 is the light-use efficiency of photosynthesis ( $mol CO_2 mol \text{ photon}^{-1}$ );  $cost$  is the cost of maintaining  
 249 leaves per unit leaf mass per day ( $g DM g DM^{-1} day^{-1}$ );  $dlen$  is day length (hour); and  $eK$  is light  
 250 attenuation coefficient at midday.

251 (4) When non-structural carbon is less than 10 g dry mass (DM) PFT<sup>-1</sup> or annual NPP is less than 10 g  
 252 DM PFT<sup>-1</sup> in the previous year, the following daily simulation processes (5--6) will be skipped.

253 (5) When total woody biomass is more than 10 kg DM, which defines the minimum tree size for  
 254 reproduction, This 10% NSC is used for every daily process of reproduction, including having flowers,  
 255 pollen, nectar, fruits, and seeds. ~~10% of non-structural carbon is transformed into litter.~~

256 (6) During the simulation of trunk growth, the remaining non-structural carbon ~~structural carbon~~ is  
 257 allocated to sapwood biomass. There is no direct allocation to heartwood, which is transformed slowly  
 258 from sapwood biomass.

259 For grass PFTs biomass, the densities of all organs comprising the biomass never decline below 0.1 g  
 260 DM m<sup>-2</sup> even if the environment is deteriorated for grass survival. A more detailed description of SEIB-  
 261 DGVM is given by Sato et al. (2007).

262

263 ~~Terrestrial water availability represents a significant source of variability in the ecosystem carbon cycle~~  
 264 ~~(Humphrey et al., 2021; Humphrey et al., 2018; Ma et al., 2021).~~ To control plant phenology and the rate  
 265 of photosynthesis as a function of the limitation in terrestrial water, the physiological status of the  
 266 limitation of terrestrial water is calculated as:

$$267 \quad p_{sat} = PMAX ce_{tmp} ce_{co_2} ce_{water} \quad (6)$$

$$268 \quad ce_{water} = \sqrt{stat_{water}} \quad (7)$$

269

$$270 \quad stat_{water} = \frac{\max(pool_{w(1)}/Depth_{(1)}, pool_{w(2)}/Depth_{(2)}) - W_{wilt}}{W_{fi} - W_{wilt}} \quad (8)$$

271 where  $p_{sat}$  is the single-leaf photosynthetic rate of tree PFTs and grass PFTs ( $\mu\text{mol CO}_2 \text{ m}^{-2} \text{ s}^{-1}$ );  
 272  $PMAX$  is the potential maximum of photosynthetic rate ( $\mu\text{mol mol}^{-1} \text{ CO}_2 \text{ m}^{-2} \text{ s}^{-1}$ );  $ce_{tmp}$  and  $ce_{co_2}$  are  
 273 the temperature and CO<sub>2</sub> concentration effect coefficient (dimensionless), separately;  $ce_{water}$  is the  
 274 water effect coefficient (dimensionless);  $stat_{water}$  is the physiological status of the terrestrial water  
 275 limitation, which ranges between 0.0–1.0, dimensionless;  $pool_{w(n)}$  is the water content in soil layer n,  
 276 mm;  $Depth_{(n)}$  is the depth of the soil layer n, mm;  $W_{wilt}$  is soil moisture at the wilting point, m  
 277 m<sup>-1</sup>; and  $W_{fi}$  is soil moisture at field capacity, m m<sup>-1</sup>. When the temperature of all soil layers is less  
 278 than 0°C,  $stat_{water}$  is equal to 0.

### 279 ~~2.3.2 Carbon stock~~ **Carbon stock** partitioning method

280 ~~According to the flexible allocation scheme,~~ SEIB-DGVM allocates and stores the biomass carbon in  
 281 four pools of woody PFT (foliage, trunk, root, and stock) and three pools of grass PFT (foliage, root, and  
 282 stock). To investigate the fractional variability of carbon sequestration potential between the pools, we  
 283 partitioned potential vegetation carbon stocks based on the physiological function of the plant (Figure  
 284 A1). ~~The root-shoot ratio (R/S) has been used to distinguish and investigate the ratio of below-ground~~  
 285 ~~biomass (root biomass) and above-ground biomass (shoot biomass) The root shoot ratio (R/S) has been~~  
 286 ~~widely used to investigate the relationship between aboveground vegetation biomass to belowground~~

287 ~~vegetation biomass and is considered an important variable in the terrestrial ecosystem carbon cycle~~  
 288 (Zhang et al., 2016). ~~–~~In this study, we adjusted the method of calculating the R/S ratio by distinguishing  
 289 between the ~~aboveground~~light-gathering vegetation biomass ~~carbon stock~~carbon stock (ALVBC) and  
 290 the ~~water-gathering~~belowground vegetation biomass ~~carbon stock~~carbon stock (BVBC/WVBC). AVBC  
 291 LVBC represents the biomass carbon invested by plant is used to gather sunlight, including ~~ing~~es biomass  
 292 carbon from woody foliage, woody trunk, and grass foliage, ~~;~~ while BVBC/WVBC represents biomass  
 293 carbon used to gather water, including ~~ing~~es biomass carbon from woody fine roots and grass fine roots,  
 294 excluding the stock pool. Stock biomass is used for foliation after dormant phase and after fires in PFTs,  
 295 which is reserve resource in each individual tree. ~~–~~Fine root biomass is just a tiny fraction to the total  
 296 biomass, but is has a very high turnover rate and determines the capacity of vegetation to absorb soil  
 297 water. Thus,

$$298 \frac{GAVBC}{WBVBC} = \frac{Wmass_{leaf} + Wmass_{trunk} + Gmass_{leaf}}{Wmass_{root} + Gmass_{root}} \times 100\% \quad (79)$$

299 where AGVBC is aboveground vegetation biomass ~~carbon stock~~carbon stock (kg C m<sup>-2</sup>); BWVBC is  
 300 belowground vegetation biomass ~~carbon stock~~carbon stock (kg C m<sup>-2</sup>); Wmass<sub>leaf</sub> is the leaf  
 301 biomass ~~carbon stock~~carbon stock of wood (kg C m<sup>-2</sup>); and Wmass<sub>trunk</sub> is the trunk biomass ~~carbon-~~  
 302 ~~stock~~carbon stock of wood (kg C m<sup>-2</sup>), including both branch and structural roots. This biomass is  
 303 simplistically attributed to aboveground organs and is used primarily to support the plant. Gmass<sub>leaf</sub>  
 304 is the leaf biomass ~~carbon stock~~carbon stock of grass (kg C m<sup>-2</sup>); whereas Wmass<sub>root</sub> and  
 305 Gmass<sub>root</sub> are functional root (fine roots) biomass carbon ~~stocks~~ of wood and grass, separately (kg C  
 306 m<sup>-2</sup>), which absorb water and nutrition from soil.

## 307 2.4 Experimental design

### 308 2.4.1 Setup of model runs

309 SEIB-DGVM simulations begin with seeds of selected ~~plant function type~~PFTs planted in bare ground.  
 310 The establishment of PFTs seeds are determined by the climatic conditions in each grid cell. The plant  
 311 ~~functional types are favored for establishment by the environmental conditions in each grid cell.~~ We  
 312 inputted the transient climate data from 1901 to 1915 to spin up the model in a repetitive loop. No obvious  
 313 trend in climatic factors was observed during this period (Tei et al., 2017). A spin-up period of 1050  
 314 years was necessary to bring the terrestrial vegetation carbon cycle into a dynamic equilibrium. To reach

315 quasi-equilibrium in the vegetation biomass, about 1000 years of simulation was required as a spin-up  
 316 procedure.

317 **2.4.2 Factorial simulation scheme**

**Table 1.** List of factorial simulations used in this study

Factorial simulation	CO <sub>2</sub> <del>fertilization</del> <u>concentration</u>	Precipitation	Temperature	Radiation	Other drivers
S1	√	√	√	√	√
S2	√				
S3	√	√			
S4	√		√		
S5	√			√	
S6	√				√

Note: In factorial simulation S1, historical atmospheric CO<sub>2</sub> concentration and historical climate fields from the CRU data set were used. In simulation S2, only historical atmospheric CO<sub>2</sub> concentration was used, and climate variables of the transient period (1901–1915) were repeatedly input. In simulation S3 (or S4, S5), only historical atmospheric CO<sub>2</sub> concentrations and precipitation (or temperature, radiation) were input, and climate variables of the transient period (1901–1915) were repeatedly input. In the last simulation S6, historical atmospheric CO<sub>2</sub> concentrations and other climate variables were input, including wind velocity and relative humidity.~~In the last simulation S6, historical atmospheric CO<sub>2</sub> concentrations and other climate variables were input, excluding precipitation, temperature, and radiation.~~

318 In order to further quantify the relative contributions of varying atmospheric CO<sub>2</sub> concentrations,  
 319 precipitation, temperature, radiation, and other factors, we performed six factorial simulations. Other  
 320 factors included wind velocity and relative humidity, which had remarkable effects on the change in  
 321 vegetation carbon stock at zonal scale. In simulation S1, atmospheric CO<sub>2</sub> concentration and all of  
 322 climate variables were varied. In simulation S2, only atmospheric CO<sub>2</sub> concentration was varied, and  
 323 climate variables were held constant (Climate variables of the transient period (1901-1915) were  
 324 repeatedly inputted). In simulation S3 (or S4, S5), atmospheric CO<sub>2</sub> and precipitation (or temperature,  
 325 radiation) were varied, and other climate variables were held constant. In simulation S6, atmospheric  
 326 CO<sub>2</sub>, wind velocity, and relative humidity were varied, and other climate variables were held constant.  
 327 Finally, S2 was used to evaluate the effects of CO<sub>2</sub> fertilization on carbon stock variation. The differences  
 328 of S2-S3, S2-S4, S2-S5, and S2-S6 were used to evaluate the response of carbon stock growth to  
 329 precipitation, temperature, radiation, and other drivers, respectively.~~To further quantify the relative~~  
 330 ~~contributions of varying atmospheric CO<sub>2</sub> concentrations, precipitation, temperature, and radiation, we~~  
 331 ~~performed six factorial simulations after the spin up procedure using different input variables between~~

332 ~~1916 and 2015 (Table 1). Other drivers included wind velocity and relative humidity. Consistent with~~  
333 ~~previous studies (Zhu et al., 2016; Piao et al., 2006), the contribution of CO<sub>2</sub> to the trend in carbon stocks~~  
334 ~~trend was defined as the ratio of the carbon stock increase from simulation S2 to that of simulation S1.~~  
335 ~~The contributions of precipitation, temperature, radiation, and other factors were calculated by~~  
336 ~~subtracting simulation S2 from each corresponding simulation (S3, S4, S5, S6, respectively), then~~  
337 ~~dividing by simulation S1.~~

### 338 2.4.3 Non-parametric test methods

339 Each driving factor (atmosphere CO<sub>2</sub>, precipitation, temperature, and radiation) has a different influence  
340 on the ~~carbon stock~~carbon stock, so it is difficult to make a simple pre-assumption about the population  
341 distribution pattern for factorial simulations. We used the non-parametric Mann-Kendall and Sen's slope  
342 estimator statistical tests (Gocic and Trajkovic, 2013) to assess the ability of SEIB-DGVM to simulate  
343 the response patterns of carbon-~~sequestration~~ storage potential to a change in climate and CO<sub>2</sub>  
344 concentrations. We regressed the simulated hundred-year mean global average ~~carbon stock~~carbon stock  
345 time series to reveal the accumulative influences of the single variables based on the factorial simulations  
346 where only one or two drivers were varied. ~~As shown in Figures A2, 3, D~~detection trends of ~~AVBC~~  
347 LVBC and BVBC-WVBC for all driving factors performed statistically well (in agreement at the 95%  
348 confidence intervals), indicating this analytical method was suitable for trend attribution at the global  
349 scale.

### 350 2.4.4 Distinguishing hydrological ~~region~~regions

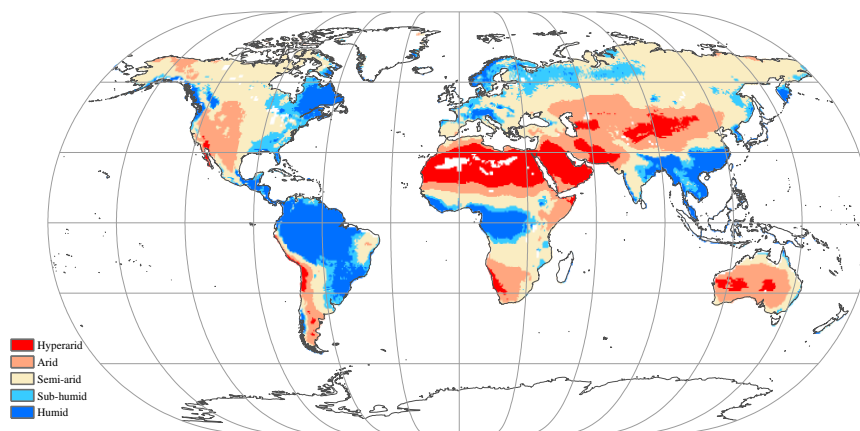


Figure 1. Global spatial patterns of water availability. Spatial variations in water availability were

categorized based on a 115-year average aridity index (AI), defined as the ratio of the multiyear mean precipitation to the potential evapotranspiration. Categories include: hyper-arid ( $AI \leq 0.05$ ), arid ( $0.05 < AI \leq 0.2$ ), semi-arid ( $0.2 < AI \leq 0.5$ ), sub-humid ( $0.5 < AI \leq 0.65$ ), and humid ( $AI > 0.65$ ).

Locally available water strongly regulates and limits the response of carbon stocks to changes in climate and CO<sub>2</sub>. We defined an aridity index (AI) to distinguish between the global hydrological regions for comparing the long-term trend in carbon stocks over different hydrological environments, and for quantifying the influences of each hydrological environment on the variations in the trends. The AI was defined as:

$$AI = \frac{\bar{P}}{\overline{ET_p}} \quad (8.10)$$

where  $\bar{P}$  is the multiyear mean precipitation (mm year<sup>-1</sup>); and  $\overline{ET_p}$  is the multiyear mean potential evapotranspiration (mm year<sup>-1</sup>), which was calculated by the Penman-Monteith model (Monteith and Unsworth, 1990). As in a previous study (Chen et al., 2019), five hydrological regions (Figure 1) were categorized based on a 115-year average AI (1901–2015): including a hyper-arid region ( $AI \leq 0.05$ ), arid region ( $0.05 < AI \leq 0.2$ ), semi-arid region ( $0.2 < AI \leq 0.5$ ), sub-humid region ( $0.5 < AI \leq 0.65$ ), and humid region ( $AI > 0.65$ ).

## 2.5 Observation dataset for model evaluation

A global time series of potential vegetation carbon was modelled by the SEIB-DGVM between 1916-2015. (R1.18) In terrestrial vegetation biomes, there is a high correlation between biomass carbon stock density and NPP per unit (Erb et al., 2016; Kindermann et al., 2008) (Figure A1). Thus, we collected NPP observation dataset and used NPP as a proxy of the carbon stock to assess model accuracy.

Ecosystem Model-Data Intercomparison (EMDI) builds upon the accomplishments of the original worldwide synthesis of NPP measurements and associated model driver data prepared by Global Primary Production Data Initiative. We obtained the monitoring station dataset from the Ecosystem Model-Data Intercomparison (EMDI) working group, and then compared their data with modelled multiyear average NPP in the period of 1916-1999 (Figure 2).

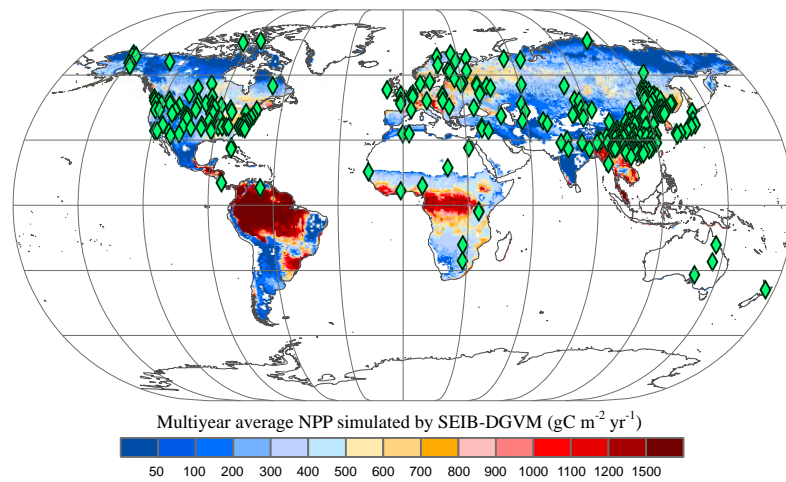


**Figure 2. Multiyear average NPP simulated by SEIB-DGVM and EMDI global site distribution.**

Green rhombuses indicate the monitoring stations of the EMDI.

374 However, *in-situ* observations are sparse for global spatial-temporal validation. Therefore, we used the  
 375 MOD17A3 products to further verify the simulated potential NPP in the twenty first century. These data  
 376 were collected by the Moderate Resolution Imaging Spectroradiometer and are some of the most widely  
 377 used data to assess the accuracy of global model simulations (Gulbeyaz et al., 2018). The natural  
 378 vegetation zones refer to the hypothetical condition that would prevail in an assumed absence of  
 379 anthropogenic activity, but under historical climate fields (Erb et al., 2018; Haberl et al., 2014). The  
 380 potential NPP is defined as that assimilated carbon stored in natural vegetation without the disturbance  
 381 of anthropogenic activities (Erb et al., 2018).

382 In order to distinguish the distribution of vegetation zones without anthropogenic disturbance, we  
 383 obtained global land cover types in the period 2001-2015 from MCD12C1 (Table A1). It was defined as  
 384 vegetation grid that the land cover type of this grid is evergreen needleleaf forest, evergreen broadleaf  
 385 forest, deciduous needleleaf forest, deciduous broadleaf forest, mixed forest, closed shrublands, open  
 386 shrublands, woody savannas, savannas or grasslands. Grid covered by other 7 land types was defined as  
 387 non-vegetation grid. Then, we calculated the proportion of each land cover types in corresponding 0.5°  
 388 grid unit. The land cover type of grid unit was determined by the max proportion among 17 land cover  
 389 types. (R2.8) Part of grids covered by grassland were grazed by livestock, leading to the decrease of NPP  
 390 of grass PFTs. We obtained land-use forcing data from Land-Use Harmonization (LUH2) to map the  
 391 distribution of managed pasture data from 2001 to 2015 (Hurtt et al., 2020). As shown in Figure A4,  
 392 grassland in eastern Asia, western Europe, south central Africa, and western South America were

393 severely affected by grazing. To exhibit the disturbance of managed pasture, we calculated the mean  
394 fraction of managed pasture within the corresponding 0.5° grid unit. When the fraction of managed  
395 pasture over 0.01, the grid covered by grassland was considered to be affected by managed pasture. We  
396 filtered grassland affected by pasture to map the distribution of natural vegetation zones without  
397 anthropogenic disturbance (Figure A5).

### 398 **3 Results and discussion**

#### 399 **3.1 Evaluation of SEIB-DGVM**

400 The EMDI dataset is an ensemble from global ecological sites from 1901 to 1999 and is shown inFigure  
401 23 illustrates the comparison between model simulated and observed multi-year mean NPP during 1916-  
402 1999. The determined coefficient ( $R^2$ ) between EMDI observed and estimated multiyear average NPP of  
403 669 *in-situ* observations is 0.54, which is significant at the  $p=0.01$  level. The slope of the regressed line  
404 is 0.70 during the twentieth century.

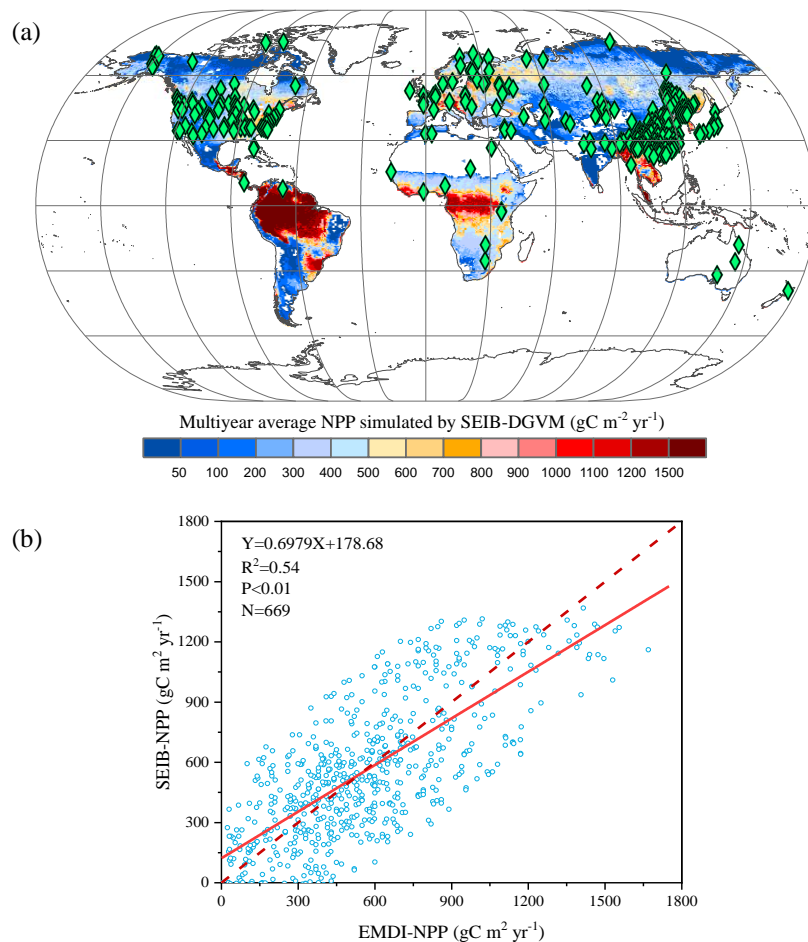




**Figure 23. Comparison of multiyear average NPP calculated by SEIB-DGVM and EMDI for the twentieth century.** (a) EMDI global site distribution. Green rhombuses indicate the locations of the sites. (b) Comparison of NPP calculated by SEIB-DGVM and EMDI. The solid line is the best fit curve; and the dashed line represents a perfect correspondence in the results of the two.

405 Based on land cover types dataset from 2001 to 2015, we obtained NPP-MOD17A3 data in natural  
406 vegetation zones without anthropogenic disturbance at the same period. However, *in situ* observations  
407 are sparse for global spatial temporal validation. Therefore, we used the MOD17A3 products to further  
408 verify the simulated potential NPP from 2000 to 2015. These data were collected by the Moderate  
409 Resolution Imaging Spectroradiometer and are some of the most widely used data to assess the accuracy  
410 of global model simulations (Gulbeyaz et al., 2018). The potential vegetation refers to the hypothetical  
411 condition that would prevail in an assumed absence of anthropogenic activity, but under historical climate  
412 fields (Erb et al., 2018; Haberl et al., 2014). The potential NPP in the potential vegetation is defined as  
413 that the assimilated carbon stored in land vegetation without human disturbance under current  
414 environmental conditions (Erb et al., 2018). We resampled actual NPP data from MOD17A3 to a  
415 common spatial resolution (0.5°) by the majority method. Potential NPP MOD17A3 data were extracted  
416 from typical NPP values in grids only covered by vegetation from actual NPP MOD17A3 data. Regions  
417 covered by undisturbed vegetation were distinguished from a land vegetation cover map. Figure 3-4  
418 shows that the modelled NPP from the SEIB-DGVM exhibited a high degree of consistency with the  
419 NPP-MOD17A3 data in natural vegetation zones over the period ( $R^2=0.62$ 0.63,  $p<0.05$ ).—The general  
420 spatiotemporal agreement between the simulated NPP derived from SEIB-DGVM with *in-situ*  
421 observations and derived from satellites reveals that it is reasonable to use the SEIB-DGVM simulations  
422 to evaluate the same mechanisms controlling global potential biomass carbon stocks of vegetation.

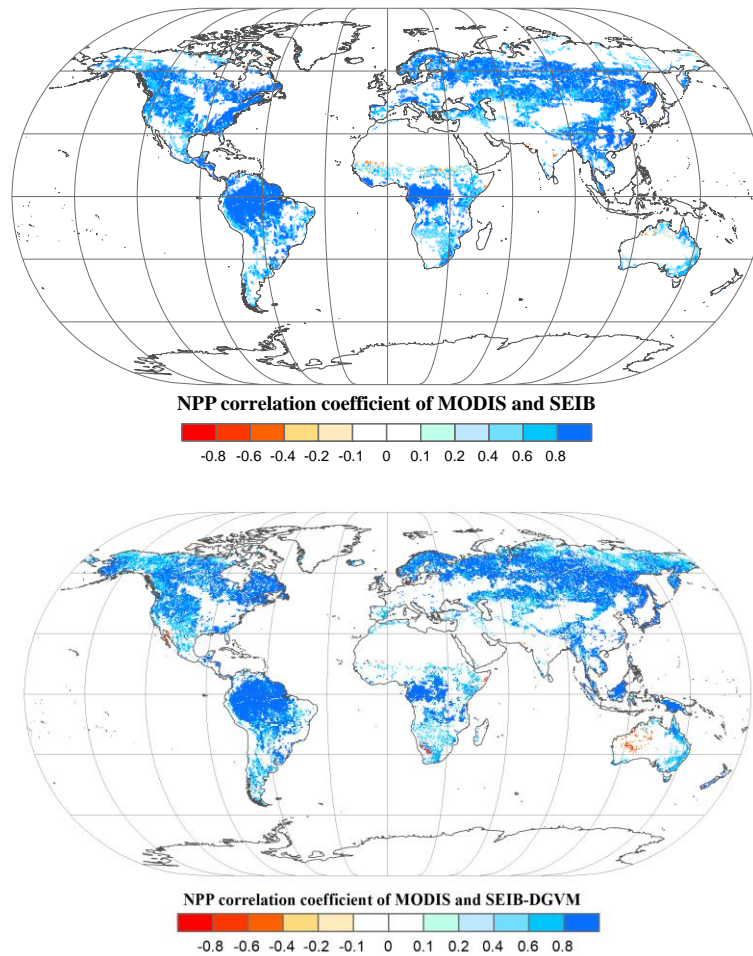


**Figure 34.** Spatial patterns in the potential NPP correlation coefficients between SEIB-DGVM and MODIS between 2001–2015. These data were used to validate SEIB-DGVM.

423 ~~For obtaining potential NPP MOD17A3 data, we collected a land use dataset from MCD12C1 to make~~  
 424 ~~a vegetation cover map in the period of 2001–2015. We resampled the land cover map to a common~~  
 425 ~~spatial resolution (0.5°), and extracted grids of covered vegetation to produce the land vegetation cover~~  
 426 ~~map (Figure A2). Cover types on the map include evergreen needleleaf forests, evergreen broadleaf~~  
 427 ~~forests, deciduous needleleaf forests, deciduous broadleaf forests, mixed forests, closed shrublands, open~~  
 428 ~~shrublands, woody savannas and grasslands.~~

429

430 Finally, the modelled result of potential vegetation biomass ~~carbon stock~~carbon stock was compared  
 431 with current existing data ~~form~~from the literature and state-of-the-art datasets. ~~–~~ Figure 4-5 shows that  
 432 the modelled results are within the range of potential carbon ~~–~~stocks, which indicate that the SEIB-  
 433 DGVM reliably simulated the ~~carbon stock~~carbon stock dynamics. ~~–~~

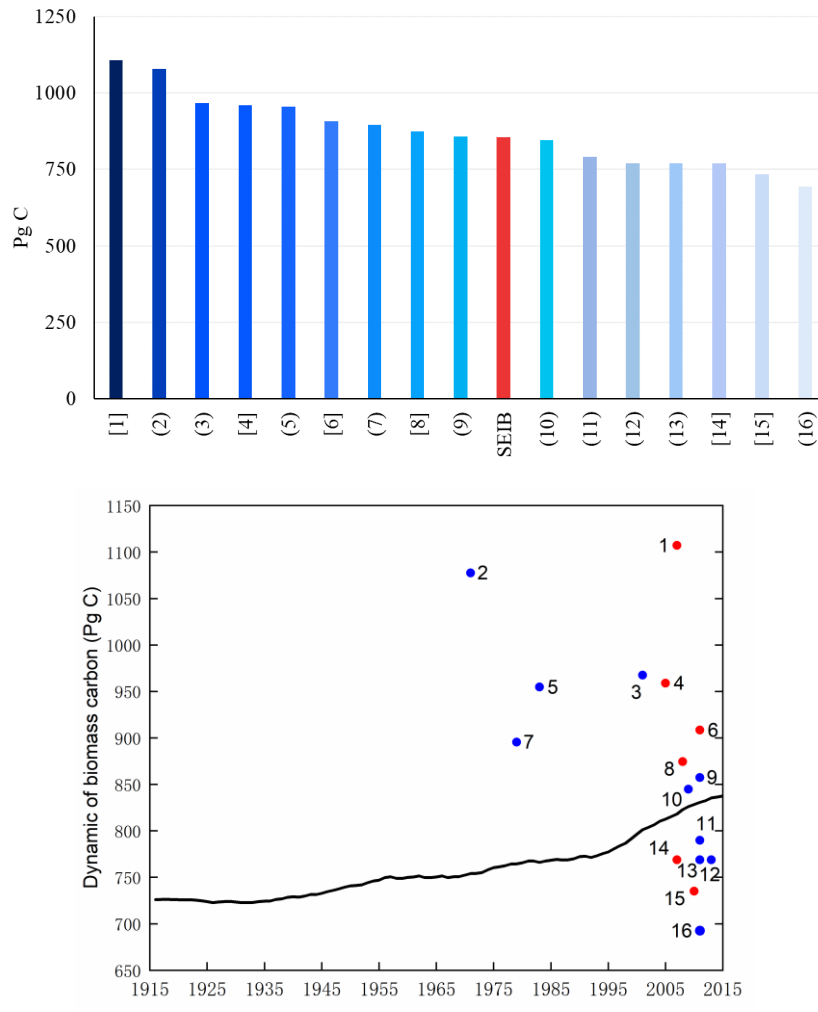


**Figure 45.** Estimates of the potential vegetation biomass carbon stock from the literature (parentheses blue plot), state-of-the-art datasets (brackets red plot) and this study (black line). Datasets are from the following studies: (1)(Erb et al., 2018; Erb et al., 2007), (2)(Bazilevich et al., 1971), (3)(Saugier et al., 2001), (4)(Erb et al., 2018; Bartholome and Belward, 2005), (5)(Olson et al., 1983), (6)(Erb et al., 2018; Pan et al., 2011), (7)(Ajtay et al., 1979), (8)(Erb et al., 2018; Ruesch and Gibbs, 2008), (9)(Kaplan et al., 2011), (10)(Shevliakova et al., 2009), (11)(Kaplan et al., 2011), (12)(Pan et al., 2013), (13)(Prentice et al., 2011), (14)(Erb et al., 2018; Erb et al., 2007), (15)(Erb et al., 2018; West et al., 2010), (16)(Hurtt et al., 2011). The red column is the SEIB-DGVM modelled biomass carbon stocks used in this study.

### 434 3.2 Enhanced carbon stocks and its fractions

435 A global time series of potential vegetation carbon stocks and its partitioning fractions were modelled  
 436 by the SEIB-DGVM between 1916-2015. The simulations were conducted at a spatial resolution of 0.5°

437 ~~and at a daily timescale using CRU and reconstructed atmospheric CO<sub>2</sub> concentration data.~~ We  
438 distinguished the changes of ALVBC and BWVBC from integral total vegetation carbon stocks. The  
439 historical temporal trends over the period are shown in Figure 56a. The potential vegetation ~~carbon-~~  
440 ~~stock~~carbon stock ~~(the year to year accumulation of carbon in the terrestrial plant without external~~  
441 ~~interference)~~ exhibits a net increase of  $119.26 \pm 2.44$  Pg C in the last century ( $\pm 2.44$  represents intra-  
442 annual fluctuation in carbon stock, which is the difference between maximum value and a minimum  
443 value of carbon stock within the year~~monthly fluctuation in carbon within the year~~). Based on Pearson  
444 correlation analysis, ~~T~~his increasing trend of annual average carbon stock exhibits a robust agreement  
445 with the ~~slower-dramatic~~ increase in atmospheric CO<sub>2</sub> concentration ( $R^2=0.889677$ ,  $p<0.001$ ), suggesting  
446 that the ~~carbon stock~~carbon stock is strongly affected by CO<sub>2</sub> fertilization. ~~In addition~~Meanwhile, the  
447 positive correlation between the ~~carbon stock~~carbon stock and CO<sub>2</sub> generally extends across ~~all~~  
448 ~~vegetation biomass partitions~~LVBC ( $R^2=0.9669$ ) and WVBC ( $R^2=0.9622$ )~~(AVBC+BVBC)~~. After the  
449 value of the global terrestrial ~~carbon stock~~carbon stock and trends were partitioned among the vegetation  
450 functional classes, we see that ALVBC increases  $116.18 \pm 2.34$  Pg C (or  $\sim 15.60\%$ ), which explains 97.42%  
451 of total carbon stock increasing trend ~~and dominates the positive global~~ ~~carbon stock~~carbon stock trend;  
452 BWVBC also increases  $3.08 \pm 0.14$  Pg C (or  $\sim 18.03\%$ ) over the past century.

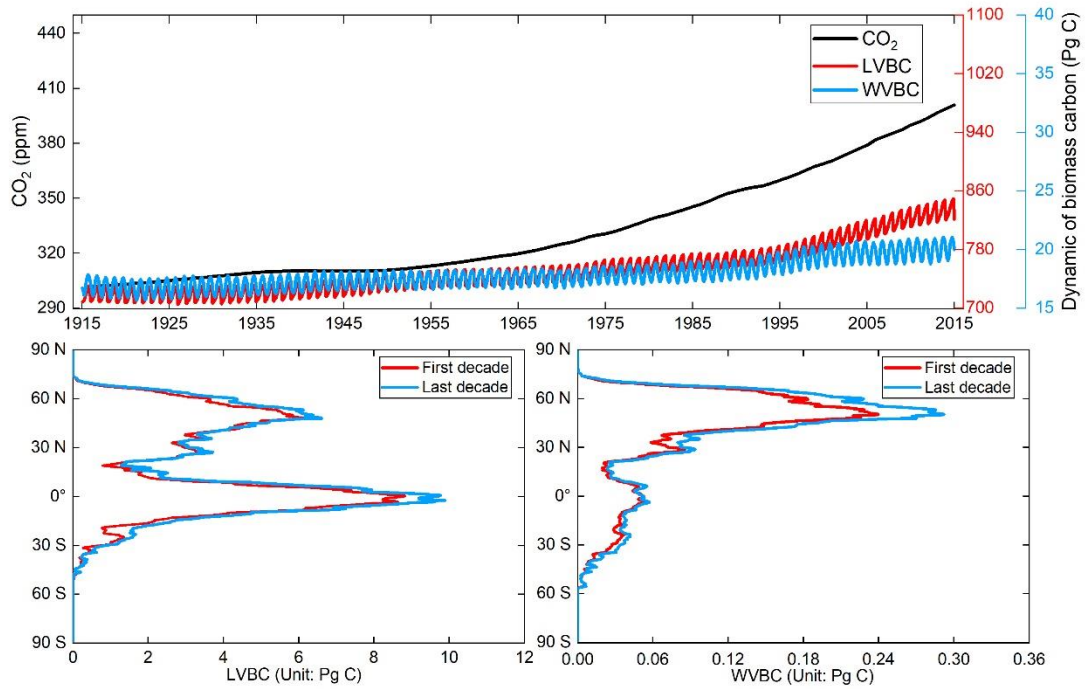
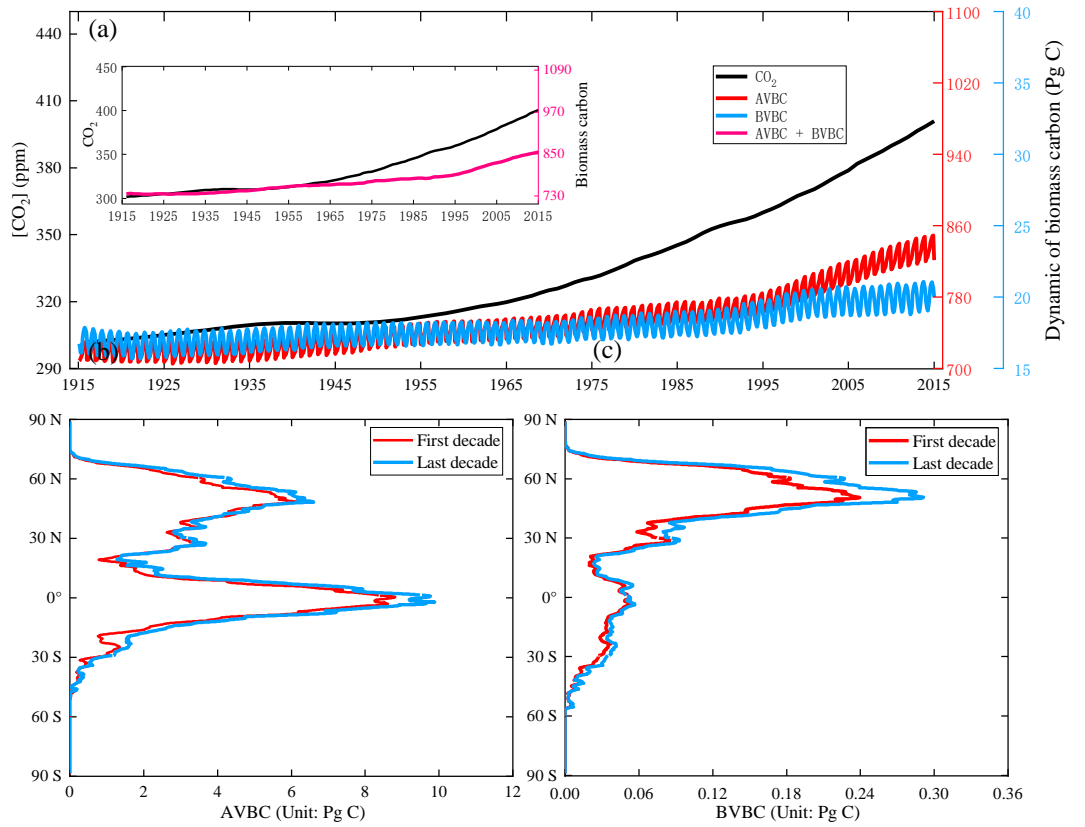


**Figure 56.** Global potential biomass carbon stocks of vegetation during the past 100 years. (a) The evolution of global potential biomass stocks ( $AVBC+LVBC+BVBC+WVBC$ ), along with changes in biomass stocks that can be attributed to the variability and trend of  $AVBC-LVBC$  and  $BVBC$

WVBC through the twentieth century. The red line represents the monthly value of AVBC-LVBC, the blue line represents the monthly value of BVBC-WVBC, and the black line represents the annual value of CO<sub>2</sub> concentration and the pink line represents the annual value of potential vegetation carbon stock.

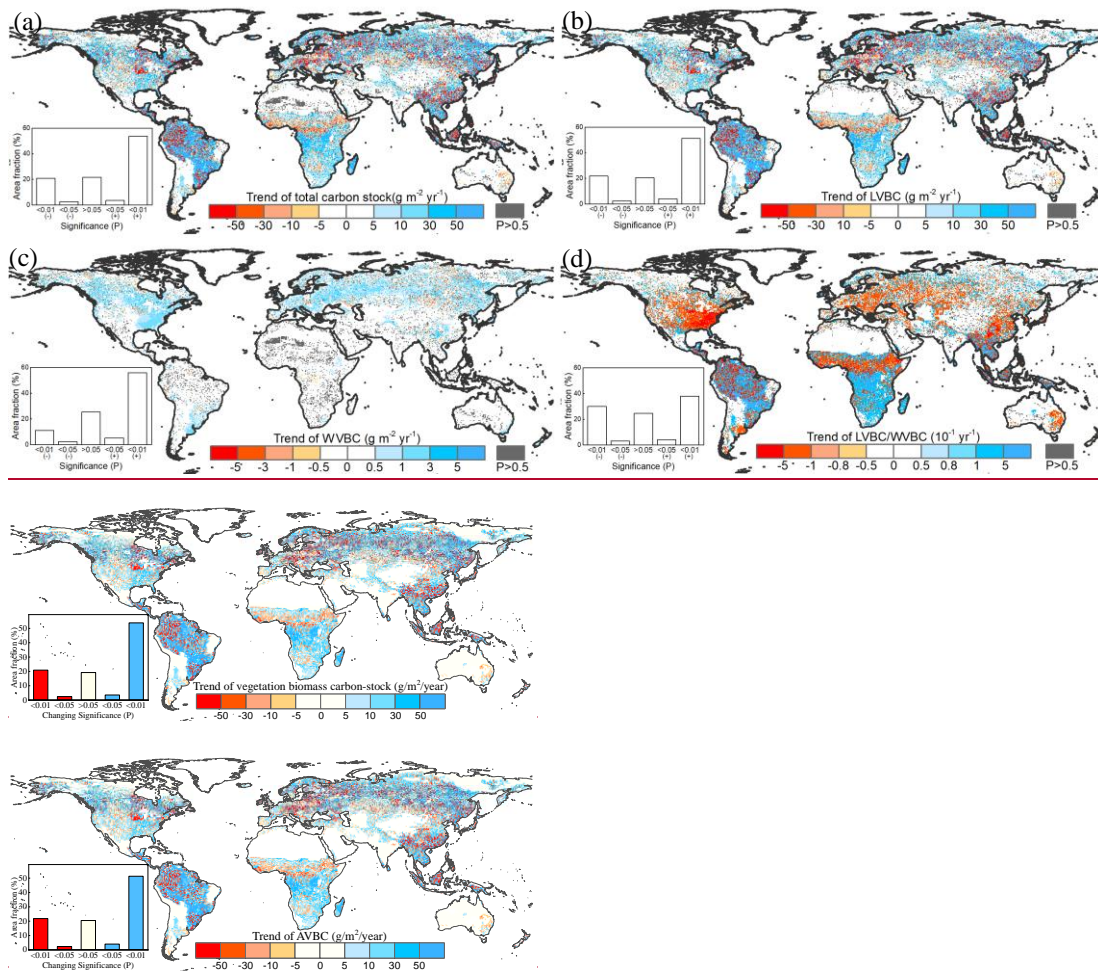
(b, c) Zonal averaged sums of the annual AVBC-LVBC and BVBC-WVBC for latitudinal bands during the first decade; ~~the averaged value~~ (1916–1925, red line) and the last decade ~~averaged value~~ (2006–2015, blue line) shows the increased carbon stock capacity.

453 The global distributions of the decadal-average change in AVBC-LVBC and BVBC-WVBC are shown  
454 in Figures 5b-6b and 5e6c, respectively. The significant historical changes in climate and CO<sub>2</sub> enhance  
455 the ~~carbon-stoek~~carbon stock of the terrestrial ecosystem, and their positive influences are broadly  
456 distributed across a latitudinal north–south gradient. The latitudinal bands of increasing annual AVBC  
457 LVBC are mainly distributed in the tropical –and boreal latitudes, ~~a conclusion consistent with prior~~  
458 ~~knowledge (Erb et al., 2018; Schimel et al., 2015)~~. The decadal and inter-annual variabilities of AVBC  
459 LVBC are dominated by the tropical and semi-arid regionzones where large portions of the regionzones  
460 are highly productive (Ahlstrom et al., 2015; Poulter et al., 2014). Tropical LVBC dominates the long-  
461 term trend of global LVBC in the last hundred years. Compared with LVBC, the increase of tropical  
462 WVBC is light. There is a single peak in the spatial variation of annual BWVBC (Figure 5e6c). BWVBC  
463 exhibits robust growth at most latitudes, and ~~it~~ increases mainly in boreal latitudes. –

### 464 3.3 Spatial variability in estimated AVBC-LVBC and BVBC-WVBC trends

465 In Figures 7(a) and 7(b), total carbon stock and LVBC exhibit a significantly increasing trend in eastern  
466 South America, southern Africa, and northern Asia, while declined in central North America, northwest  
467 South America, and central Africa. WVBC showed a more widely increasing tendency in North America,  
468 southeastern South America, and Europe, while had a decrease trend in part zones of Asian. W~~Based on~~  
469 ~~the carbon stock partitioning method, we found~~ find that the ~~integrated total carbon-stoek~~carbon stock  
470 as well as the ~~above~~light- and ~~belowgroundwater-gathering vegetation biomass~~ carbon-stocks over the  
471 period of 1916–2015 exhibited a remarkable spatial heterogeneity. –Figure 6a-7a shows that an increase  
472 in vegetation carbon-stocks occurred over regionzones and global aggregate levels during the entire  
473 study period. About 57.39% of the terrestrial grids exhibited an increase with a noticeable trend ( $p < 0.05$ )  
474 in biomass ~~carbon-stoek~~carbon stock; 53.82% of global grids possessed increases that were statistically  
475 significant at the  $p = 0.01$  level. To determine the contributions of each fraction (AVBC-LVBC,

476 BVBCWVBC) to the integral-total change in the potential vegetation carbon-stockcarbon stock, we  
 477 partitioned and present the historical spatial and temporal patterns for each fraction separately (Figure  
 478 6b7b, 6e7c). AVBC-LVBC contributes 97.33% to the total-incremental change of total carbon stock  
 479 ( $116.18 \pm 2.34$  Pg C), with about 51.32% of the grids possessing a noticeable positive trend ( $p=0.01$ ).  
 480 Generally, spatial patterns of AVBC-LVBC and the integral-total carbon-stockcarbon stock are consistent  
 481 (Figure 6a7a, 6b7b), which further supports the argument that AVBC-LVBC dominates the trend in  
 482 carbon-\_stocks in most regionzones. Although the proportion of the total change in carbon-\_stocks is  
 483 small (2.58% of total carbon stock increase $3.08 \pm 0.14$  Pg C), -about 61.00% of the land surface shows  
 484 an increase in BVBCWVBC; of these terrestrial grids, 55.81% was characterized by a significant  $p=0.01$   
 485 increase.



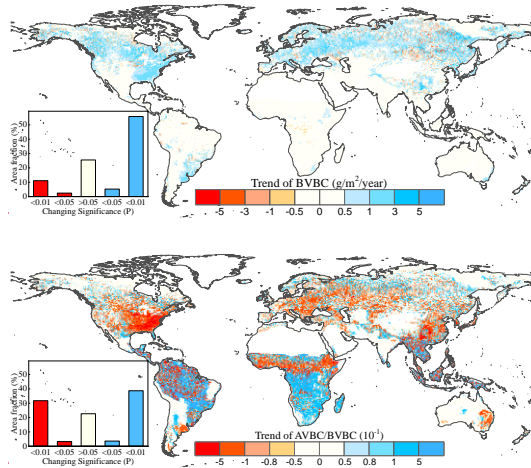


**Figure 67.** Spatial patterns in the trends of potential vegetation carbon stocks and their fractions from 1916 to 2015. Difference induced by changes in climate and CO<sub>2</sub> in terrestrial biomass carbon stock (a), AVBC-LVBC (b), and BVBC-WVBC (c) during the historic period 1916–2015. The blue bar indicates the significantly increasing trends and the red bar indicates the significantly decreasing trends in carbon stocks. (d) Trend in the AVBC/LVBC/BVBC-WVBC ratio from 1916 to 2015. The sub-graphs show the significant test results. The white bar indicates non-vegetated areas, or the trend is statistically insignificant (P>0.05). The blue bar indicates significantly increasing trends in the ratio, and vice versa. The grey bar indicates the trend is statistically insignificant (P >0.05). The sub-graphs show the significant test results. A '+' symbol indicates a positive trend, and vice versa.

486 Biomass carbon allocation between above and belowground vegetation organs reflect the changes in  
 487 individual growth, community structure and ecosystem function, which are important attributes in the  
 488 investigation of carbon stocks and carbon cycling within the terrestrial biosphere (Hovenden et al., 2014;  
 489 Fang et al., 2010; Ma et al., 2021). Under the influences of a changing climate and CO<sub>2</sub> concentrations,  
 490 there is a slight increase in the ratio of global AVBC/LVBC/BVBC/WVBC; the rate of increase is 0.0171  
 491 yr<sup>-1</sup> in the last hundred years, which is significant at the 0.01 level (Figure 647d). About 42.08% of the  
 492 terrestrial grids exhibited an increase with a noticeable trend (p<0.05) in the ratio of LVBC and WVBC;  
 493 37.95% of global grids possessed increases that were statistically significant at the p=0.01 level.  
 494 Meanwhile, 33.32% of the land surface shows a significant decrease in LVBC/WVBC; of these terrestrial  
 495 grids, 30.06% was characterized by a significant p=0.01 decrease. RegionZones with noticeable increases  
 496 in the ratio of AVBC-LVBC to BVBC-WVBC are mainly located in southern Africa, central South



497 America, and northern Eurasia. Negative trends in AVBC-LVBC/BVBC-WVBC ratios are found in  
498 northern America, southern Europe, and tropical Africa.–

#### 499 **3.4 Responses of AVBC-LVBC and BVBC-WVBC to environmental drivers**

500 The responses of AVBC-LVBC and BVBC-WVBC to changes in climate and CO<sub>2</sub> are both positive at  
501 the global level (Figure 7a8a, 7e8c), although regionalzonally, they exhibit both negative and positive  
502 responses (Figure 7b8b, 7d8d). Based on the results of factorial simulations and Mann-Kendall+Sen tests,  
503 CO<sub>2</sub> fertilization explains the largest proportion of the change in the carbon stockcarbon stock–; about  
504 82.45% change in AVBC-LVBC was positive (15.521 g C m<sup>-2</sup> yr<sup>-1</sup>Figure 8a), whereas 89.28% of the  
505 change in BVBC-WVBC was positive (0.435 g C m<sup>-2</sup> yr<sup>-1</sup>Figure 8c). In factorial simulation S2, the long-  
506 term trend of LVBC was 15.521 g C m<sup>-2</sup> yr<sup>-1</sup> and that of WVBC was 0.435 g C m<sup>-2</sup> yr<sup>-1</sup> at the period  
507 from 1916 to 2015 (Figure A2a and Figure A3a). The separately simulated AVBC-LVBC and BVBC  
508 WVBC increased by 80.98 Pg C and 2.66 Pg C with increasing atmospheric CO<sub>2</sub> concentrations (from  
509 301.73 ppm in 1916 to 400.83 ppm in 2015). The other climatic drivers (precipitation, temperature,  
510 radiation, humidity, and wind speed) remained at baseline values. While the increase or decrease in the  
511 carbon stockcarbon stock may be attributed to more than one driving factor, within any specified grid,  
512 the one with the highest contribution was the driver that consistently resulted in the highest increase or  
513 decrease in the carbon stockcarbon stock for that grid. The spatial pattern illustrates that CO<sub>2</sub> dominates  
514 the variability in AVBC-LVBC in 7.28% of the regionzones, including 1.21% of the regionzones that  
515 exhibited a negative change and 6.07% that exhibited a positive change (Figure 8b). CO<sub>2</sub> dominates the  
516 variability in BVBC-WVBC in 27.60% of the regionzones, including 1.73% of the regionzones that  
517 exhibited a negative change and 25.87% of regionzones with a positive change (Figure 7b, 7d8d). Under  
518 the effect of CO<sub>2</sub> fertilization, grids with increased trend in WVBC mainly distribute in boreal latitudes  
519 (Figure 6c). –These trends are consistent with and previous studies (Tharammal et al., 2019; Zhu et al.,  
520 2016; Keenan et al., 2017) in which positive trends occurred, especially for BVBCWVBC. The responses  
521 of terrestrial ecosystems to high CO<sub>2</sub> concentration are affected by vegetation species and the dynamic  
522 function of the vegetation carbon stock. Due to the interaction between terrestrial vegetation and a  
523 changing environment, both photosynthesis and respiration of the vegetation also changed. To better  
524 absorb CO<sub>2</sub> and sunlight required for photosynthesis, vegetated regions are gradually covered by  
525 vegetation with higher plant height and wider leaf area, thereby adjusting their characteristic ecosystem

526 functions (Anderson et al., 2010) (Figure 6d). Fractional dynamics of the carbon stock (AVBC/BVBC)  
 527 are widely used as a key indicator to investigate the responses of vegetation to environmental drivers,  
 528 which also reflect the response strategies of vegetation in environments with different water limitations  
 529 (Yang et al., 2010).

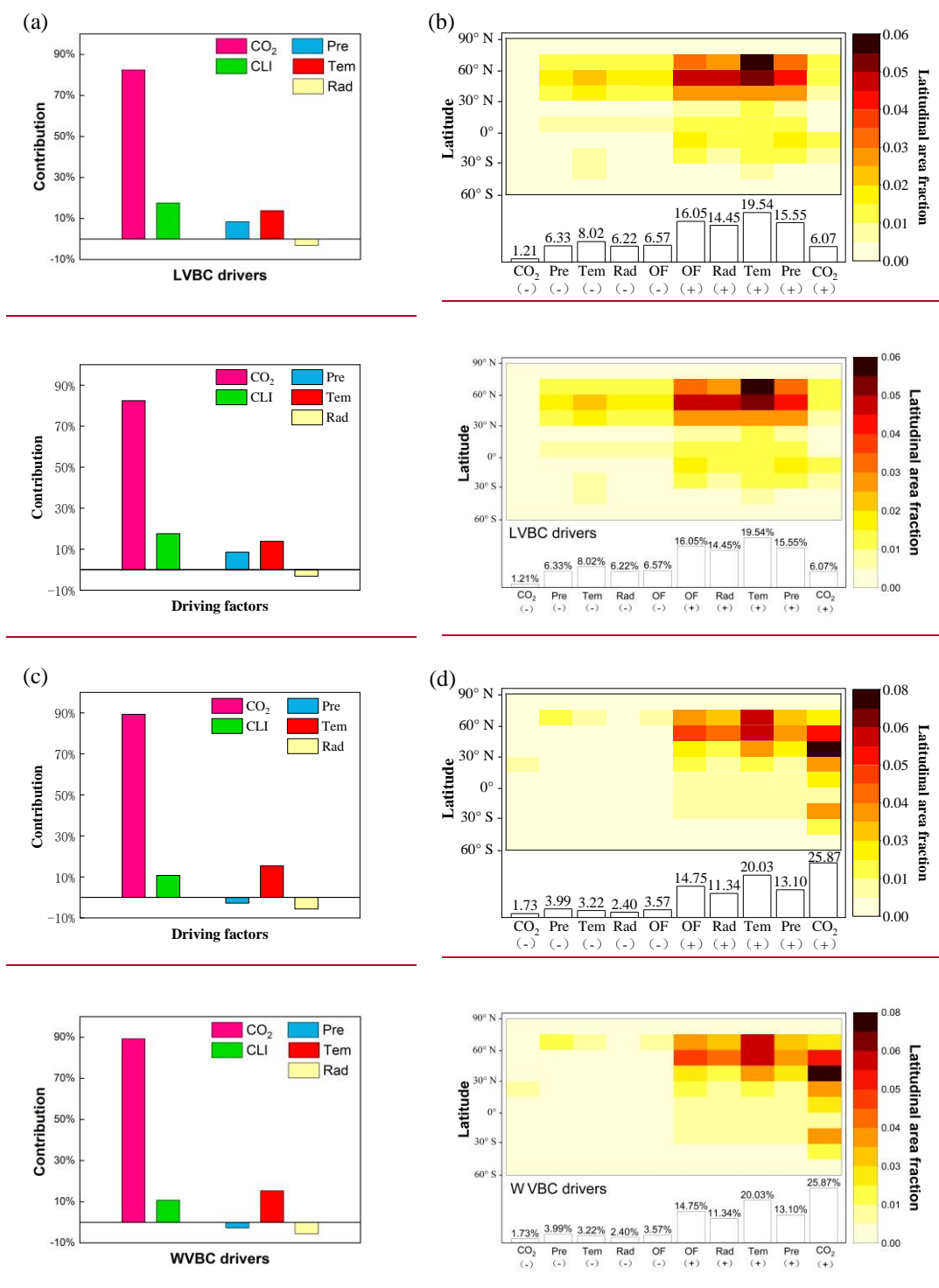
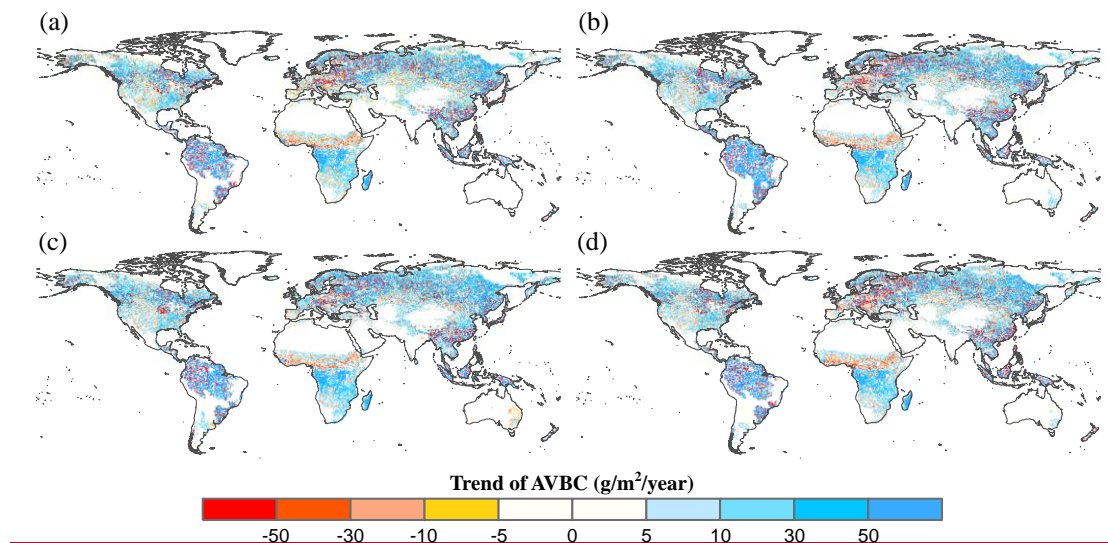


Figure 78. The proportion of change in the integrated-vegetation biomass carbon stocks

**attributed to driving factors.** Ratios of the driving factors of CO<sub>2</sub> fertilization effects (CO<sub>2</sub>), climate change effects (CLI), precipitation (Pre), temperature (Tem), radiation (Rad) for AVBC-LVBC (a) and BWVBC (c) under the five scenarios using the Mann-Kendall and Sen's slope estimator statistical tests. Attribution of ALVBC (b) and BWVBC (d) dynamics to driving factors calculated as averages along 15° latitude bands. At local scales, the driving factors include CO<sub>2</sub>, Pre, Tem, Rad, and other climate factors (OF). A '+' symbol indicates a positive effect of the driving factor on carbon stock, and vice versa. The fraction of global area (%) that is predominantly influenced by the driving factors is shown at the top of the bar.

530 Climate change induced by the greenhouse effect explains part of the increase in carbon stocks, but  
531 unlike CO<sub>2</sub> fertilization, climate has dramatic negative effects on some vegetated regionzones. Figure 7  
532 8a illustrates that temperature is the largest climatic contributor to the change in AVBC-LVBC (13.83%,  
533 2.572 g m<sup>-2</sup> yr<sup>-1</sup>), followed by precipitation (8.51%, 1.572 g m<sup>-2</sup> yr<sup>-1</sup>) and radiation (-3.19%, -0.649 g  
534 m<sup>-2</sup> yr<sup>-1</sup>). The spatial distribution shows that temperature predominantly influences the change in  
535 AVBCLVBC (Figure 8b), influencing over 27.56% of the global vegetated regionzones, followed by  
536 precipitation (21.88%) and radiation (20.67%). Figure 8c shows there is a difference in the negative  
537 contribution of precipitation to the change in WVBC at the global level (-2.76%, -0.013 g m<sup>-2</sup> yr<sup>-1</sup>).  
538 Temperature is the largest climatic contributor to the change in WVBC (15.36%, 0.075 g m<sup>-2</sup> yr<sup>-1</sup>),  
539 followed by radiation (-5.63%, -0.027 g m<sup>-2</sup> yr<sup>-1</sup>). Modelled BVBC-WVBC trends based on the factorial  
540 simulations have similar spatiotemporal patterns to AVBCLVBC (Figures A2 and A3), the spatial  
541 patterns of light- and water-gathering carbon stocks show a significant increasing trend in the most of  
542 boreal zones. In the Southern Hemisphere, the trends of WVBC are extensively statistically insignificant  
543 in all factorial simulations, and only a small proportion of grids show a significantly increasing trend.  
544 There is a significantly increasing trend in LVBC in south-central Africa and northern South America.  
545 The effects of temperature on WVBC are stronger than LVBC, because temperature has a stronger effect  
546 on the metabolism process of root growth, dominating the turnover rate and the costs of maintenance  
547 respiration in root growth process (Gill and Jackson, 2000)The effects of temperature on BVBC are  
548 stronger than AVBC, because fine root tightly correlates with temperature (Gill, 2000). Meanwhile,  
549 there is a difference in the negative contribution of precipitation to the change in BVBC at the global  
550 level (- 2.76%, -0.013 g m<sup>-2</sup> yr<sup>-1</sup>). It should be noted that trends in the global carbon stockcarbon stock

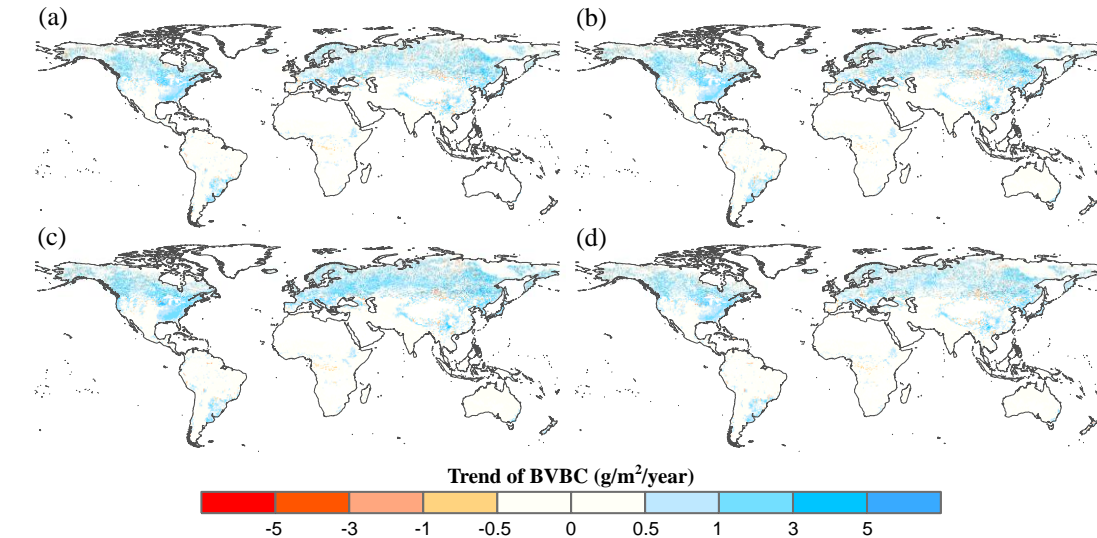
551 can be largely attributed to the influences of CO<sub>2</sub>, precipitation, temperature, and radiation (Figures 8;  
 552 9). Nonetheless, at the regionalzonal scale, the contributions of other factors should be considered, such  
 553 as humidity and wind speed. The effects of these other factors dominate trends in AVBC-LVBC in over  
 554 16.05% of the regionzones that increased and 6.57% of the regionzones that decreased. In the case of  
 555 changes in BVBCWVBC, other factors were dominant drivers in over 14.75% of the regionzones that  
 556 increased and 3.57% of regionzones that decreased. Under the effect of climate, the variability of LVBC  
 557 and WVBC is positive in most zones, promoting the noticeable increase of carbon stocks in boreal  
 558 latitudes. Previous studies have pointed out that the interannual variation of the terrestrial carbon stock  
 559 caused by releasing or sequestering carbon is sensitive to anomalous changes in water availability and  
 560 light use efficiency (Madani et al., 2020; Humphrey et al., 2018). However, multidecade observational  
 561 data revealed that there was not a dramatic and consistent variant in the land surface precipitation and  
 562 radiation data series (Sun et al., 2012; Wild et al., 2005). It appears that the influences of precipitation  
 563 and radiation on short term variations in the carbon stocks were temporally compensated for by  
 564 offsetting changes of AVBC, BVBC, and AVBC/BVBC in the long term trend. The accumulated  
 565 influence of climate warming induces dramatic changes in the carbon stock at a global scale. Thus, we  
 566 suggest that temperature dominates the long term trends in the carbon stock among climatic drivers,  
 567 while a compensatory effect exists in the long term change in the carbon stock induced by precipitation  
 568 and radiation.



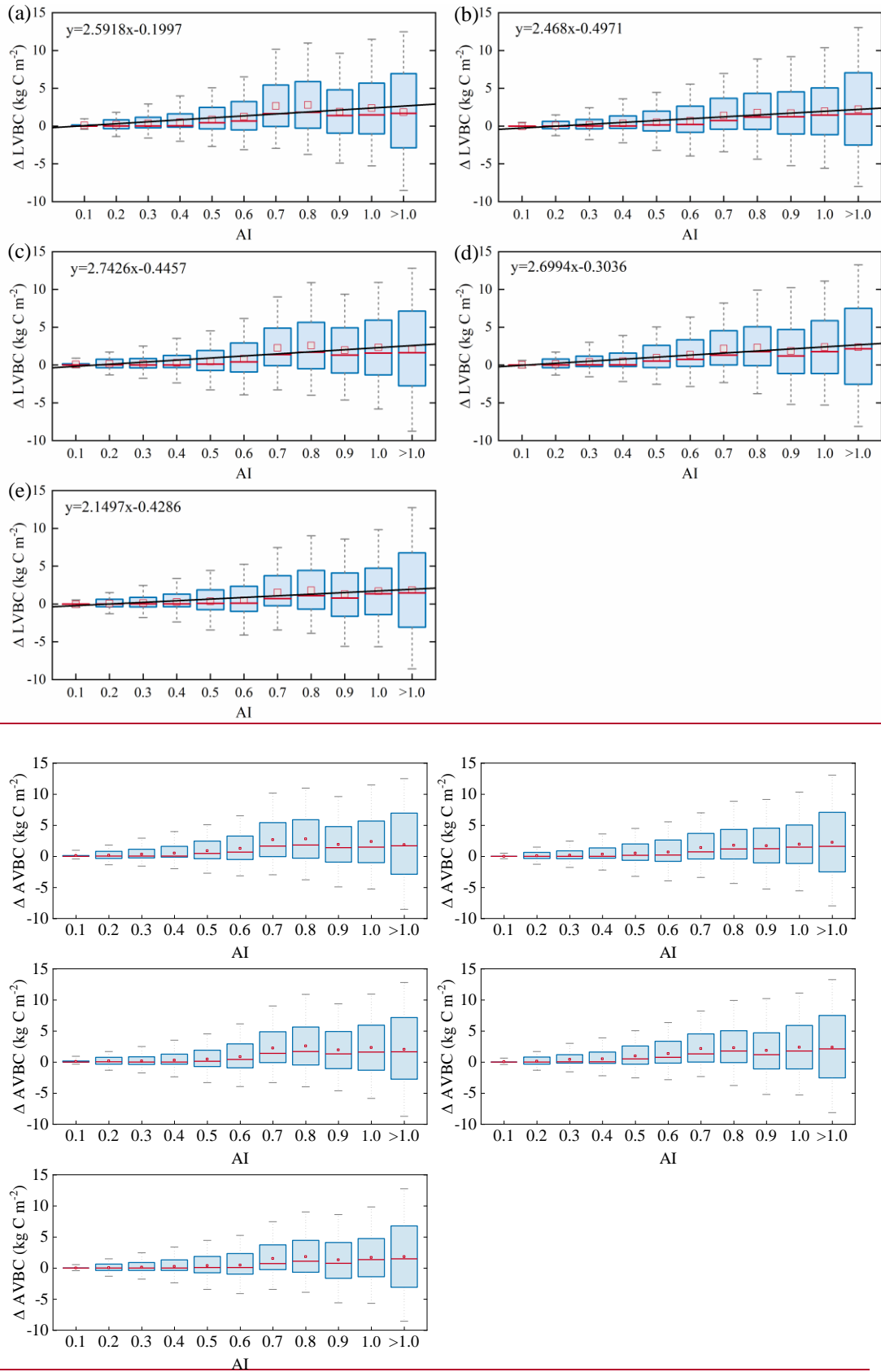
**Figure 8. Potential AVBC trend maps during the period of 1916 to 2015 under different factorial simulations. (a) CO<sub>2</sub> driving factorial simulation; (b) CO<sub>2</sub>+precipitation driving factorial simulation. (c)**

~~CO<sub>2</sub>+temperature driving factorial simulation; and (d) CO<sub>2</sub>+radiation driving factorial simulation. Positive values indicate increasing trends in the ratio and vice versa. All results from Mann-Kendall and Sen's slope statistical tests correspond to the 95% confidence interval.~~

569



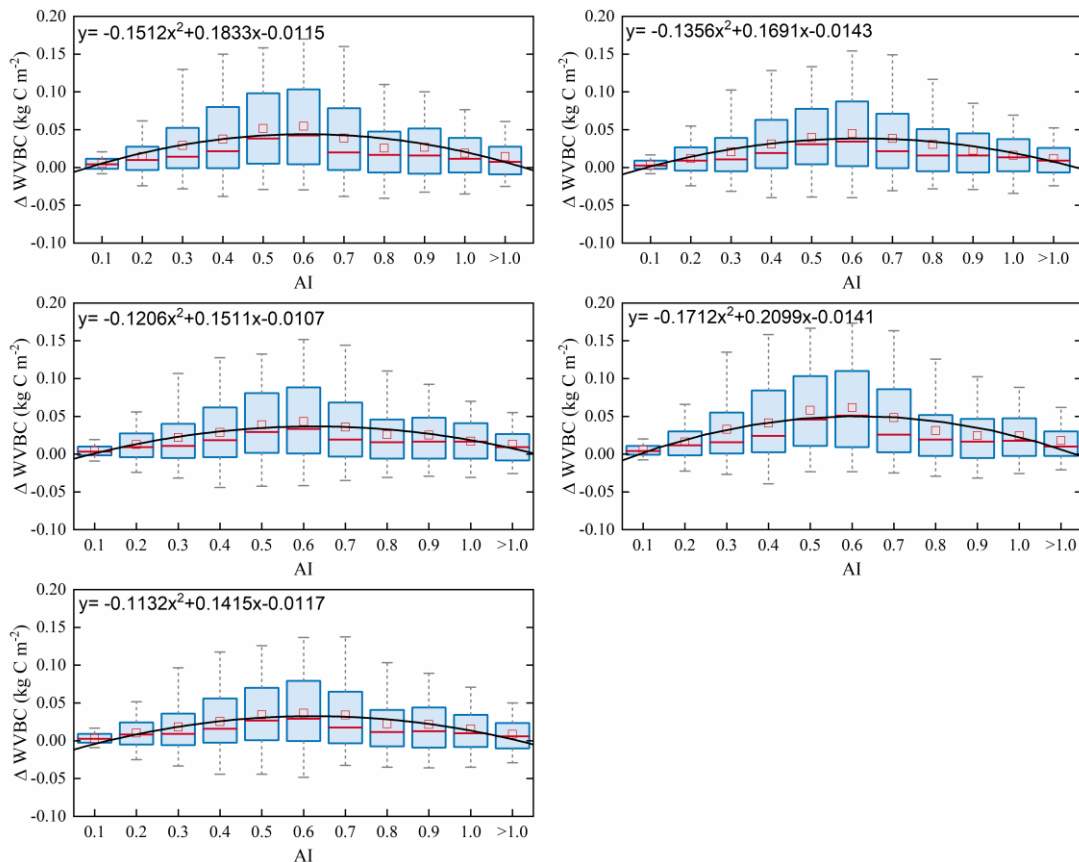
**Figure 9. Potential BVBC variation trend maps during the period of 1916 to 2015 under different factorial simulations. (a) CO<sub>2</sub> driving factorial simulation; (b) CO<sub>2</sub>+precipitation driving factorial simulation. (c) CO<sub>2</sub>+temperature driving factorial simulation; and (d) CO<sub>2</sub>+radiation driving factorial simulation. Positive values indicate increasing trends in the ratio and vice versa. All results from Mann-Kendall and Sen's slope statistical tests correspond to the 95% confidence interval.**



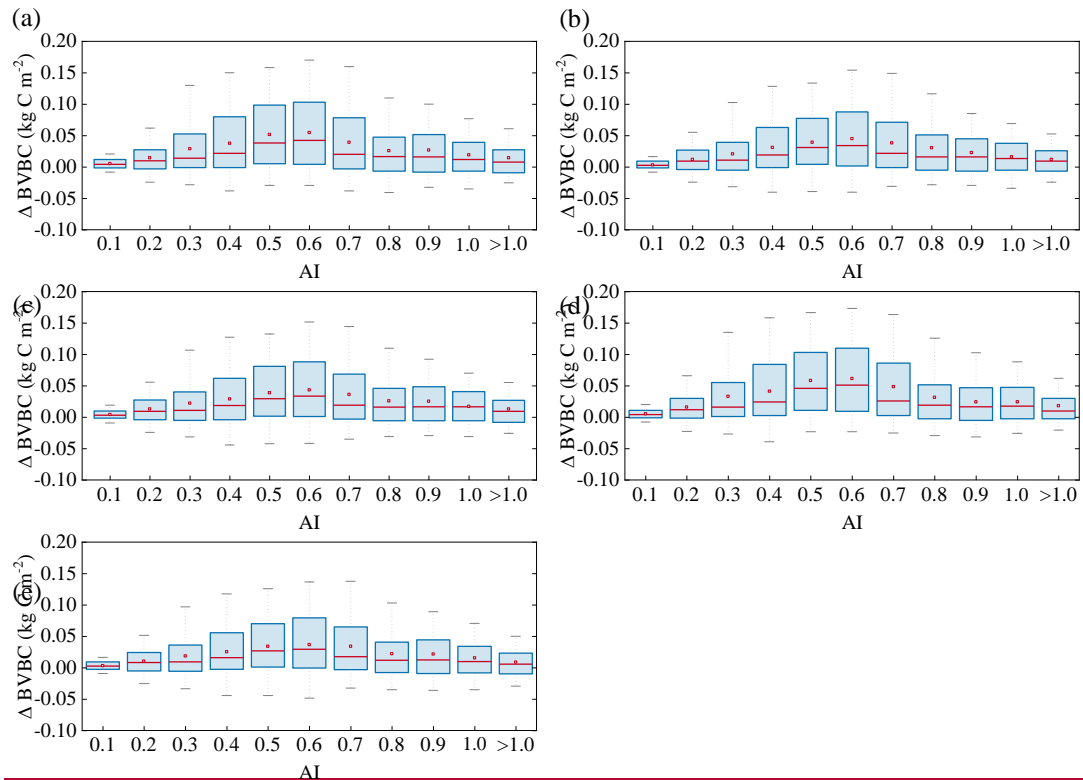
**Figure 109. Relationships in the incremental change between AI and ~~AVBC-LVBC~~ over the hydrological ~~regionz~~ones. Modelled ~~AVBC-enhanced-magnitude-Magnitude of change in LVBC~~ in the historical scenario S1 (a), CO<sub>2</sub> in scenario S2 (b), ~~CO<sub>2</sub> + precipitation~~ in scenario S3 (c), ~~CO<sub>2</sub> + temperature~~ in scenario S4 (d), and ~~CO<sub>2</sub> + radiation~~ in scenario S5 (e). Range of the box is 25%-75% of values; range of the whiskers is 10%-90% of values; the small red square is average value; ~~and~~ the red line is the median line; ~~and the black line is the fitted curve.~~ Positive value of the Y axis represents the magnitude of increased LVBC from 1916 to 2015 under water-limitations conditions, and vice versa.**

571 Terrestrial water availability emerged as a key regulator of terrestrial carbon storage, by affecting the  
 572 response mechanism of the vegetation ~~carbon-stock~~carbon stock to changes in driving factors (~~Fan et al.,~~  
 573 ~~2019; Humphrey et al., 2018; Ahlstrom et al., 2015; Madani et al., 2020; Humphrey et al., 2021; Ma et~~  
 574 ~~al., 2021~~). As shown in Figures ~~109 and 10~~, with an increase in the aridity index (i.e., an increase in  
 575 available water), the magnitude and range in variations of LVBC density and WVBC density gradually  
 576 enhance. Based on the results of factorial simulations, we find a positive relationship between LVBC  
 577 and water pressure. In extreme water stress, the increase of LVBC tends to zero and plants stop growing.  
 578 There is no obvious different in the slopes of fitting curves between factorial simulations. The pattern of  
 579 the enhanced magnitude and range of variation in the WVBC density is unimodal with water stress  
 580 gradient in all factorial simulations. With the increasing of AI, the magnitude of change in WVBC  
 581 increases at first and then decreases finally. The mitigation of water stress promotes WVBC increase,  
 582 while excess surface water limits the response of WVBC to changes in climate and CO<sub>2</sub>. there is a  
 583 gradually ascending trend in the enhanced magnitude and range in variation of AVBC density. Moreover,  
 584 there is a link between fluctuations in the enhanced magnitude and range of variation in the BVBC  
 585 density with the water stress gradient (Figure 11). These results reveal that the carbon stock increases  
 586 stimulated by changes in climate and CO<sub>2</sub> are constrained by water available. With increased warming,  
 587 water limitations are expected to increasingly limit the carbon stock increase, specially at arid  
 588 ~~regions~~ These results suggest that water limitations lessen or even prevent carbon stock fluctuations  
 589 ~~induced by changes in climate and CO<sub>2</sub>.~~ To further ~~investigate~~ reveal the controls of water limitation on  
 590 the responses of inner carbon storages to each driver, we analyse the long-term variability of potential  
 591 vegetation carbon\_~~stocks~~ by means of factorial simulations for each hydrological ~~region~~region (Figure

592 1). It is revealed in factorial simulations, from Figure A6 that the increased LVBC density induced by  
593 drivers attributed to increase AVBC density changed—from  $0.878 \pm 0.131 \text{ kg C m}^{-2}$  in the hyper-  
594 arid region to  $5.459 \pm 0.610 \text{ kg C m}^{-2}$  in the humid regions during the past hundred years.  
595 At global scale, the annual mean value of LVBC simulated by each factorial simulation is close. In hyper-  
596 arid and arid regions, the interannual change of LVBC in historical scenario matches most closely with  
597 that of S3 scenario which considers CO<sub>2</sub> and precipitation effects. Increased WVBC density induced by  
598 drivers attributed to increase BVBC density changed from  $0.011 \pm 0.001 \text{ kg C m}^{-2}$  in the hyper-  
599 arid region to  $0.044 \pm 0.005 \text{ kg C m}^{-2}$  in the humid regions during the same period (Figures  
600 A3, A74). The long-term trends of WVBC simulated by each scenario are consistent across different  
601 hydrological regions. With a lessening of water stress (from hyper-arid to humid area), the  
602 response of the carbon stock to changes in climate and CO<sub>2</sub> gradually became more  
603 noticeable. The robust pattern in the regional average density of the carbon stock  
604 shows that terrestrial water limitations strongly limit the enhanced magnitude of the carbon  
605 stock.



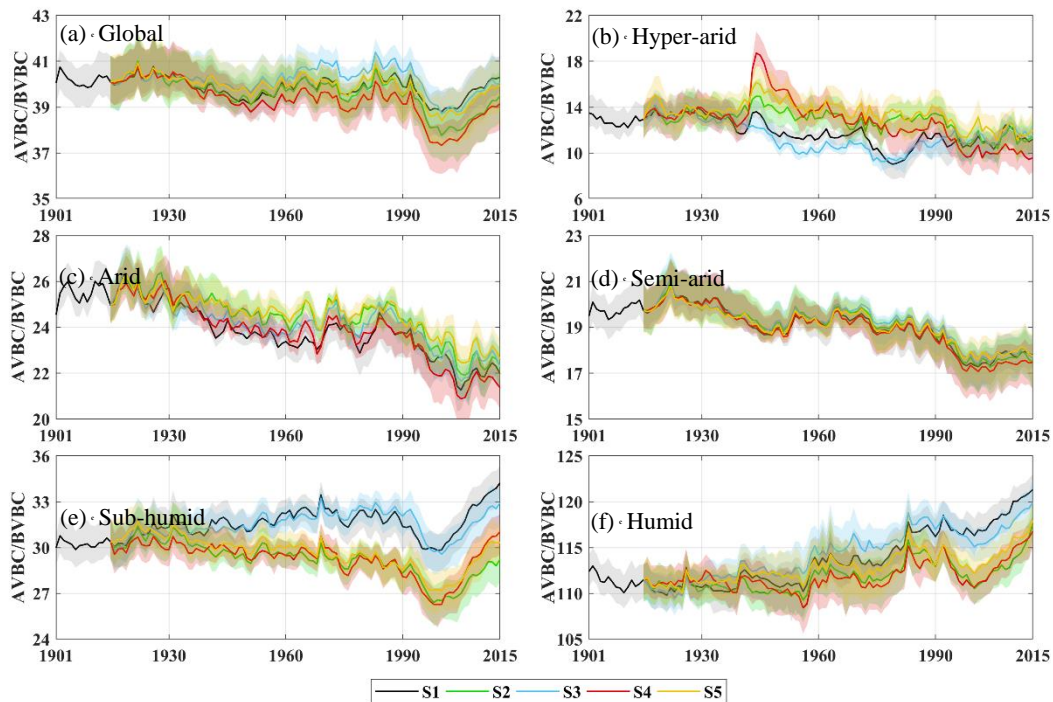




**Figure 14.10. Relationships in the incremental change in AI and  $\Delta BVBC$  over the hydrological regions.** Modelled  $\Delta BVBC$  enhanced magnitude in the historical scenario S1 (a),  $CO_2$  in scenario S2 (b),  $CO_2 +$  precipitation in scenario S3 (c),  $CO_2 +$  temperature in scenario S4 (d), and  $CO_2 +$  radiation in scenario S5 (e). Range of the box is 25%-75% of values; range of the whiskers is 10%-90% of values; the small red square is average value; and the red line is the median line, and the black line is the fitted curve. Positive value of the Y axis represents the magnitude of increased WVBC from 1916 to 2015 under water-limitations conditions, and vice versa.

606 Water limitations not only directly reduced the magnitude of the increase-response in the two fractions'  
 607 carbon-stock (AVBC-LVBC and BVBC-WVBC) to changes in climate and  $CO_2$ , but also  
 608 indirectly confined the response direction of each fractions' carbon-stock by transforming  
 609 vegetation structure and function. Figure 12.11 illustrates that spatial-temporal variations in the carbon-  
 610 stock ratio within and between hydrological regions. From hyper-arid region to humid  
 611 region, the variation range of ratio between LVBC and WVBC significantly increases. Plants store more  
 612 assimilated carbon in shoots and leaves in humid regions. The long-term effects of driver changes have  
 613 a positive influence on this carbon allocate pattern. Under the synergistic effect of drivers and water  
 614 stress, vegetation carbon-stock increases, and there is a larger proportion of biomass

615 allocated to, and stored in, aboveground light-gathering vegetation organs.— In drylands ( $AI \leq 0.5$ ) of all  
 616 factorial simulations, aboveground light- and belowground water-gathering biomass carbon stocks both  
 617 increased but the rate of change in the AVBC/LVBC/BVBC-WVBC ratio gradually decreased. To  
 618 mitigate water stress, plants allocate more assimilated carbon to root for gathering water. Vegetation  
 619 utilizes a tolerance strategy to allocate biomass, storing more biomass carbon in roots to resist enhanced  
 620 water stress (Chen et al., 2013).— In humid region zones ( $AI > 0.65$ ), the proportion of AVBC-LVBC  
 621 increases more than that of BVBC-WVBC to obtain more resources like  $CO_2$  and radiation energy,  
 622 leading to an increase in the AVBC/LVBC/BVBC-WVBC ratio. — Conforming to the optimal partitioning  
 623 hypothesis, plants store more carbon in shoots and leaves in environments where water is more available  
 624 and shift more carbon to roots when water is more limited (Yang et al., 2010; Meconnaughay and  
 625 Coleman, 1999). Terrestrial water availability has a strong regulating effect on the spatial pattern of  
 626 growth in the carbon stock, demonstrating that the effects of the changes in climate and  $CO_2$  on the  
 627 dynamics of the vegetation carbon stock are controlled by the terrestrial water gradient.



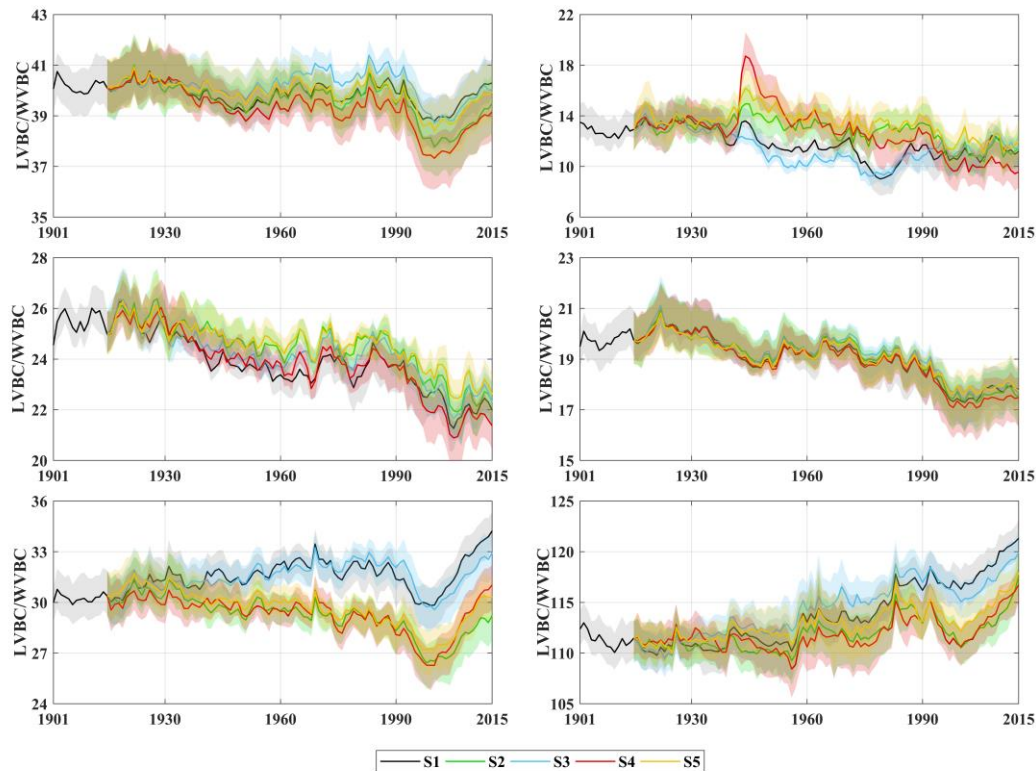


**Figure 12.11.** Temporal fluctuations in carbon-stockcarbon stock dynamics in vegetation biomass in different factorial simulations. Black indicates historical factorial simulation from 1901-2015, green indicates the CO<sub>2</sub>-driven factorial simulation, blue indicates the precipitation-driven factorial simulation, red indicates the temperature-driving factorial simulation and yellow indicates radiation driven factorial simulation. Uncertainty bounds are provided as shaded areas reflect the intra-annual fluctuation ( $\pm 1$  s.d.) (a) Modelled trend of LVBC/WVBC ratio in Global area. (b-f) Modelled trend of the LVBC/WVBC ratio in different hydrological regionregions.

628 **4 Conclusions and dDiscussions and conclusion**

629 To understand the response of carbon-sequestrationstorage potential and its inner biomass carbon-stocks  
 630 to environmental change, we conducted a series of factorial simulations using SEIB-DGVM V3.02. More  
 631 importantly, we investigated the extent of the responses of carbon-stocks to water limitations,and the  
 632 correlation between terrestrial water and carbon flux.

633

634 Over the past 100 years, there has been an ongoing increase in the carbon storage capacity of the  
 635 terrestrial ecosystem from 735 Pg C in 1916 to 855 Pg C in 2015, which has slowed the rate at which

636 atmospheric CO<sub>2</sub> has increased and may have mitigated global warming. These findings are consistent  
637 with the conclusions of research conducted at the local scale. For example, based on carbon flux data,  
638 Erb et al. (2008) suggested that the vegetation ~~carbon stock~~carbon stock in Austria increased from 1043  
639 Mt C to 1249 Mt C (~~AVBC~~aboveground carbon stocks growth was 1.059 Mt C yr<sup>-1</sup> and  
640 ~~BVBC~~belowground carbon stocks growth was 0.2 Mt C yr<sup>-1</sup>) since industrialization. Le Noë et al. (2020)  
641 showed that increases in the carbon stocks and carbon density were the predominant drivers in the forest  
642 terrestrial carbon sequestration capacity in France from 1850 to 2015. Tong et al. (2020) also found a  
643 substantial increase of ~~AVBC~~aboveground carbon stocks in southern China (0.11 Pg C yr<sup>-1</sup>) during the  
644 period 2002–2017. However, these studies focused on ~~regional~~zonal trends in ~~integral~~total vegetation  
645 carbon~~\_~~stocks and did not investigate the extent of the response in vegetation carbon~~\_~~stocks partitioned  
646 between ~~above~~light- and ~~belowground~~water-gathering biomass. Our results show that the increase in  
647 ~~carbon stock~~carbon stock in ~~aboveground~~light-gathering vegetation organs was much larger than that in  
648 ~~belowground~~water-gathering vegetation organs, and ~~AVBC~~light-gathering biomass carbon stock  
649 dominates the historical trend of the terrestrial ~~carbon stock~~carbon stock. During the past decades, the  
650 global land surface has been greening because of the flux and storage of more carbon into plant trunks  
651 and foliage (Zhu et al., 2016). Compared with WVBC, LVBC increase 116.18 ± 2.34 Pg C and dominates  
652 the long-term trends of vegetation carbon stock. The latitudinal bands of increasing annual LVBC are  
653 mainly distributed in tropical latitudes, a conclusion consistent with prior knowledge that tropical zones  
654 dominate carbon uptake and storage (Erb et al., 2018; Schimel et al., 2015). Biomass carbon allocation  
655 between light- and water-gathering vegetation organs reflect the changes in individual growth,  
656 community structure and ecosystem function, which are important attributes in the investigation of  
657 carbon stocks and carbon cycling within the terrestrial biosphere (Hovenden et al., 2014; Fang et al.,  
658 2010; Ma et al., 2021). During the past hundred years, the ratio of LVBC/WVBC shown a slight upward  
659 trend. The rate of increase is 0.0171 yr<sup>-1</sup>, which is significant at the 0.01 level. To better absorb CO<sub>2</sub> and  
660 sunlight required for photosynthesis, vegetated regions are gradually covered by vegetation with higher  
661 plant height and wider leaf area, thereby adjusting their characteristic ecosystem functions (Anderson et  
662 al., 2010).  
663  
664 Based on our factorial simulations, the vegetation ~~carbon stock~~carbon stock exhibited the most increase

665 under the ~~combined~~ influence of CO<sub>2</sub> fertilization ~~and temperature~~. In addition, the responses of carbon-  
666 stocks to ~~climatic~~ other factors of change differed, particularly at the ~~regional~~ zonal scale (Figure 78).  
667 ~~Previous studies have pointed out that the variation of the terrestrial carbon stock caused by releasing or~~  
668 ~~sequestering carbon is sensitive to anomalous changes in water availability and light use efficiency~~  
669 ~~(Madani et al., 2020; Humphrey et al., 2018). At local scale, radiation dominated the long-term trend of~~  
670 ~~LVBC in 20.67% of global zones and that of WVBC in 13.74%, while precipitation dominated the long-~~  
671 ~~term trend of LVBC in 21.88% of global zones and that of WVBC in 17.09% of global zones. However,~~  
672 ~~radiation induced light variation in LVBC (-3.19%) and WVBC (-5.62%) at global scale. Precipitation~~  
673 ~~explain 8.51% of LVBC trend and -2.76% of WVBC trend at global scale. LVBC and WVBC variations~~  
674 ~~driven by precipitation and radiation were ultimately offset by spatially compensatory effects, which~~  
675 ~~dampened the response of the carbon stock to these factors at global scale (Jung et al. 2017). Temporal~~  
676 ~~AVBC and BVBC variations driven by precipitation and radiation were ultimately offset by~~  
677 ~~compensatory effects, which dampened the long term response of the carbon stock to these factors.~~  
678 ~~Trend in temperature drove historical long-term trends in the potential carbon stocks, with faster~~  
679 ~~increases and considerable variation occurring by zone. The accumulated influence of climate warming~~  
680 ~~induces dramatic changes in the carbon stock at a global scale. Thus, our results revealed that temperature~~  
681 ~~dominates the long-term trends in the carbon stock among climatic drivers, while a compensatory effect~~  
682 ~~exists in the global change in the carbon stock induced by precipitation and radiation. Our results revealed~~  
683 ~~that trends in CO<sub>2</sub> and temperature drove historical long term trends in the potential carbon stocks, with~~  
684 ~~faster increases and considerable variation occurring by region.~~

685

686

687 By partitioning the trends of ~~AL~~LVBC and ~~BW~~WVBC into five hydrological ~~region~~ regions (Figure 1), we  
688 found that the long-term change in carbon-~~stocks~~ is tightly coupled to terrestrial water availability. These  
689 results indicate that vegetation in humid ~~region~~ regions is responsible for most of the trend in global  
690 ~~AVBC~~LVBC, while plants in semi-arid ~~region~~ regions play a dominate global role in controlling the long-  
691 term trend in ~~BVBC~~WVBC. ~~In addition, we demonstrated that water limitations controlled the terrestrial~~  
692 ~~vegetation carbon stocks (Ma et al., 2021).~~ As water stress decreases, the magnitude and range in  
693 variation of ~~carbon stocks~~LVBC gradually increase (Figures 10, 11), which suggests that limited water

694 availability constrains the response magnitude of the changes in LVBC carbon stocks to changes in CO<sub>2</sub>  
695 and climate. The response pattern of WVBC growth to the increasing water availability is different from  
696 that of LVBC. Drought mitigation promotes the growth of WVBC, while humid region with high light  
697 competition limits root growth. The result is consistent with previous finding that plants reduce allocation  
698 to roots in dense forests where aboveground competition for light is high (Ma et al. 2021). – Moreover,  
699 we found that indirect effects of water limitation regulate increasing rate of each carbon pool~~In contrast,~~  
700 ~~we found that indirect factors constrain the impact of increasing water stress on the response of carbon-~~  
701 ~~stocks.~~ – Although vegetation carbon-stocks dramatically increase under the effects of climate and CO<sub>2</sub>  
702 changes, the increasing rate of LVBC faster than WVBC in humid region. Vegetation stores more  
703 biomass in aboveground plant organs (trunk and foliage) to gather light.~~vegetation in humid regions~~  
704 ~~stores more biomass (and carbon) in aboveground plant organs (trunk and foliage) to obtain nutrients~~  
705 ~~and light.~~ Dryland vegetation decrease~~lowers~~ the ALVBC/BWVBC ratios and stores more biomass  
706 below ground to enhance the capture of water resources. Based on these results, we demonstrated that  
707 water limitations controlled the variable response of terrestrial vegetation carbon stocks. Our findings  
708 are consistent with other reports about the impact of increasing water limitations on terrestrial ecosystem.  
709 Based on satellite remote sensing observations, Madani et al. (2020) found that changes in water  
710 constraints can lead to variable responses in ecosystem productivity and net carbon exchange. Humphrey  
711 et al. (2021) found that increasing water stress limits the response magnitude of carbon uptake rates  
712 through a down-regulation of stomatal conductance and suggested that land carbon uptake is driven by  
713 temperature and vapour pressure deficit effects that are controlled by terrestrial water availability. Ma et  
714 al. (2021) found that plants increase investment into building roots in arid region because the extent of  
715 water limitation there is exacerbated by global warming. Terrestrial ecosystems utilize sensitive  
716 strategies to allocate and store biomass to adjust to local hydrological conditions,~~which is consistent~~  
717 ~~with optimal partitioning theory (Meconnaughay and Coleman, 1999).~~ – A significant conclusion is that  
718 water constraints not only confine the responses of vegetation carbon-stocks to drivers of variability, but  
719 also constrain the proportion of biomass carbon-stocks in abovegather- and belowgroundwater-gathering  
720 fractions.

721

722

723 Distinguishing the response of ~~carbon stock~~carbon stock fractions estimated by SEIB-DGVM improves  
724 the understanding of the interactive impacts of terrestrial carbon and water dynamics. However,  
725 uncertainty still exists because of the limitations in the processes of modelling vegetation metabolism  
726 with SEIB-DGVM. Trunk biomass contains tree branches and structural roots (coarse roots and tap roots)  
727 (Sato et al., 2007), so the R/S ratio of potential vegetation in factorial simulations is smaller than the R/S  
728 of actual vegetation in ~~factorial simulations~~observation stations. Root biomass only contains the fine root  
729 biomass, leading to an underestimate in belowground organ biomass of trees and grasses compare with  
730 previous conclusion (Ma et al., 2021; Yang et al., 2009). ~~Fine root biomass is just a tiny fraction to the~~  
731 ~~total biomass, but is has a very high turnover rate and determines the capacity of vegetation to absorb~~  
732 ~~soil water~~. Availability of nitrogen is a key limiting factor for vegetation growth, especially when higher  
733 CO<sub>2</sub> fertilization effects exist (Tharammal et al., 2019). The limitation could be alleviated by nitrogen  
734 deposition in most temperate and boreal ecosystems. The SEIB-DGVM experiments were conducted  
735 with a focus on documenting CO<sub>2</sub> fertilization and climate change interactions; these experiments did not  
736 consider the influences of nitrogen deposition, which leads to a slight overestimate of the contributions  
737 of CO<sub>2</sub> fertilization on biomass production.

738

739 In summary, we evaluated SEIB-DGVM V3.02 and used this model to offer new perspectives on the  
740 response of vegetation carbon ~~sequestration storage~~ potential to changes in climate and CO<sub>2</sub>. Our  
741 simulation results show that changes in CO<sub>2</sub>, rather than climate, dominate the ~~above-light- to~~  
742 ~~belowgroundwater-gathering~~ partitioning of the carbon ~~sequestration storage~~ potential. More  
743 importantly, we suggest that the impact of CO<sub>2</sub> fertilization and temperature effects on vegetation carbon-  
744 sequestration potential depends on water availability and its impacts on plant stress. With increased  
745 global warming, water limitations are expected to increasingly confine global carbon ~~sequestration~~ and  
746 storage. Our findings highlight the need to account for terrestrial water limitation effects when estimating  
747 the response of the terrestrial carbon ~~storage~~sequestration capacity to global climate change, and the  
748 need for stronger interactions between those involved in vegetation model development and those in  
749 between the hydrological and ecological research communities.

Table A1. MCD12C1 legend and class descriptions

<u>Name</u>	<u>Value</u>	<u>Description</u>
<u>Evergreen Needleleaf Forests</u>	<u>1</u>	<u>Dominated by evergreen conifer trees (canopy &gt;2m). Tree cover &gt;60%.</u>
<u>Evergreen Broadleaf Forests</u>	<u>2</u>	<u>Dominated by evergreen broadleaf and palmate trees (canopy &gt;2m). Tree cover &gt;60%.</u>
<u>Deciduous Needleleaf Forests</u>	<u>3</u>	<u>Dominated by deciduous needleleaf (larch) trees (canopy &gt;2m). Tree cover &gt;60%.</u>
<u>Deciduous Broadleaf Forests</u>	<u>4</u>	<u>Dominated by deciduous broadleaf trees (canopy &gt;2m). Tree cover &gt;60%.</u>
<u>Mixed Forests</u>	<u>5</u>	<u>Dominated by neither deciduous nor evergreen (40-60% of each) tree type (canopy &gt;2m). Tree cover &gt;60%.</u>
<u>Closed Shrublands</u>	<u>6</u>	<u>Dominated by woody perennials (1-2m height) &gt;60% cover.</u>
<u>Open Shrublands</u>	<u>7</u>	<u>Dominated by woody perennials (1-2m height) 10-60% cover.</u>
<u>Woody Savannas</u>	<u>8</u>	<u>Tree cover 30-60% (canopy &gt;2m).</u>
<u>Savannas</u>	<u>9</u>	<u>Tree cover 10-30% (canopy &gt;2m).</u>
<u>Grasslands</u>	<u>10</u>	<u>Dominated by herbaceous annuals (&lt;2m).</u>
<u>Permanent Wetlands</u>	<u>11</u>	<u>Permanently inundated lands with 30-60% water cover and &gt;10% vegetated cover.</u>
<u>Croplands</u>	<u>12</u>	<u>At least 60% of area is cultivated cropland.</u>
<u>Urban and Built-up Lands</u>	<u>13</u>	<u>At least 30% impervious surface area including building materials, asphalt, and vehicles.</u>
<u>Cropland/Natural Vegetation Mosaics</u>	<u>14</u>	<u>Mosaics of small-scale cultivation 40-60% with natural tree, shrub, or herbaceous vegetation.</u>
<u>Permanent Snow and Ice</u>	<u>15</u>	<u>At least 60% of area is covered by snow and ice for at least 10 months of the year.</u>
<u>Barren</u>	<u>16</u>	<u>At least 60% of area is non-vegetated barren (sand, rock, soil) areas with less than 10% vegetation.</u>
<u>Water Bodies</u>	<u>17</u>	<u>At least 60% of area is covered by permanent water bodies.</u>
<u>Unclassified</u>	<u>255</u>	<u>Has not received a map label because of missing inputs</u>



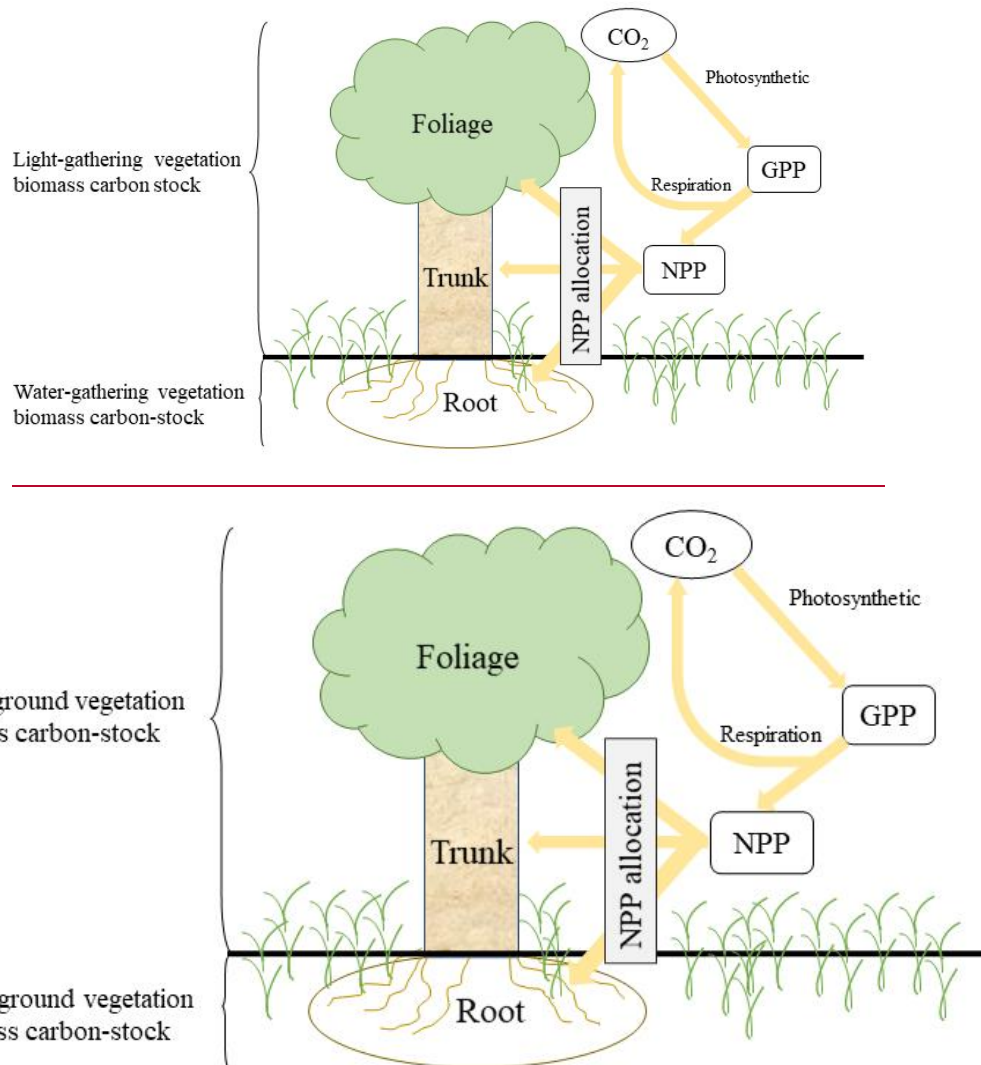
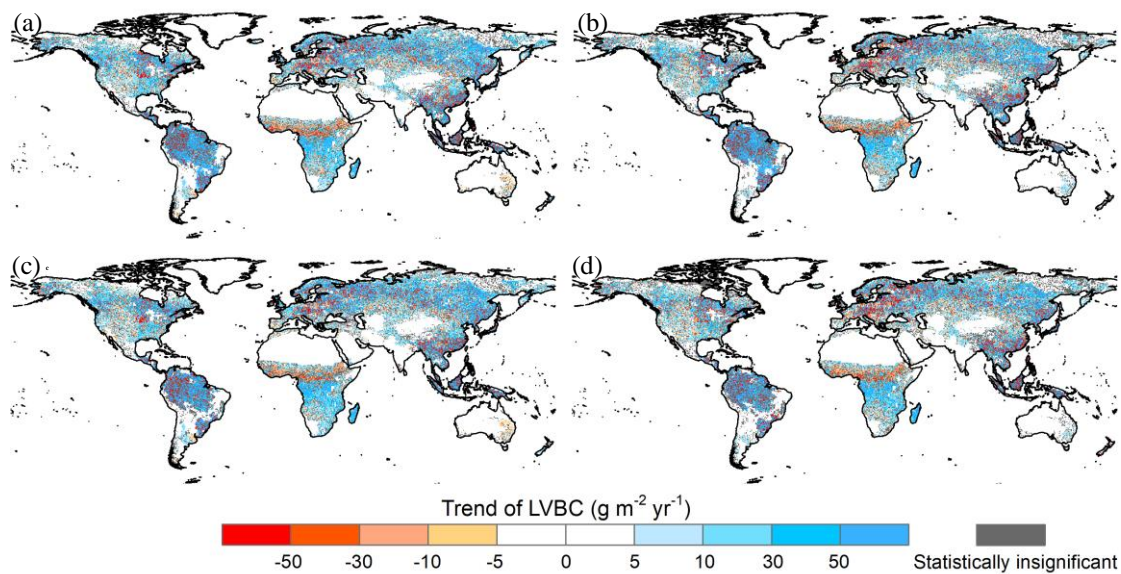
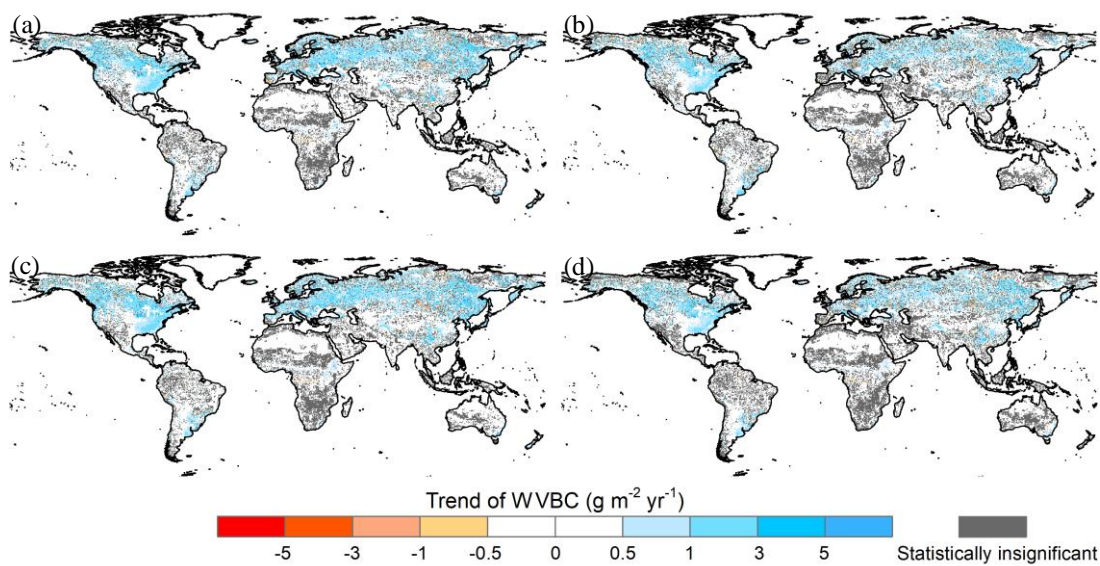


Figure A1. Schematic of ecosystem carbon cycle. Yellow arrow indicates carbon flux. Atmospheric  $CO_2$  transitions into gross primary production (GPP) by photosynthesis. GPP is partitioned into respiration and net primary production (NPP). NPP is partitioned into three biomass carbon pools (foliage, trunk, and root).



**Figure A2. Potential LVBC trend maps during the period of 1916 to 2015 under different factorial simulations.** (a) CO<sub>2</sub> driving factorial simulation; (b) CO<sub>2</sub>+precipitation driving factorial simulation. (c) CO<sub>2</sub>+temperature driving factorial simulation; and (d) CO<sub>2</sub>+radiation driving factorial simulation. Positive values indicate increasing trends in the ratio, and vice versa. All results from Mann-Kendall and Sen's slope statistical tests correspond to the 95% confidence interval.

754



**Figure A3. Potential WVBC variation trend maps during the period of 1916 to 2015 under different factorial simulations.** (a) CO<sub>2</sub> driving factorial simulation; (b) CO<sub>2</sub>+precipitation driving factorial simulation. (c) CO<sub>2</sub>+temperature driving factorial simulation; and (d) CO<sub>2</sub>+radiation driving factorial simulation. Positive values indicate increasing trends in the ratio, and vice versa. All results

from Mann-Kendall and Sen's slope statistical tests correspond to the 95% confidence interval.

755

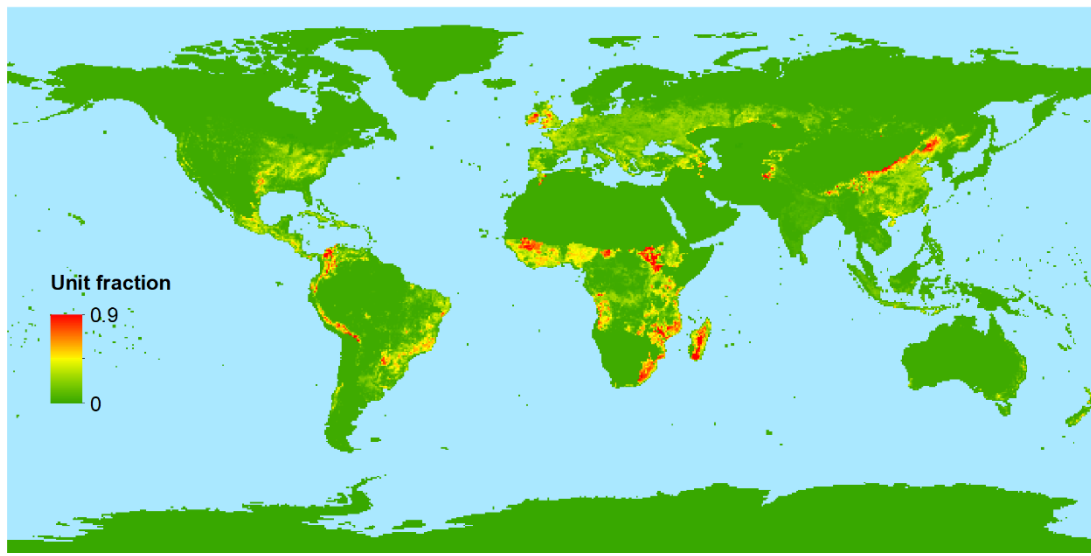
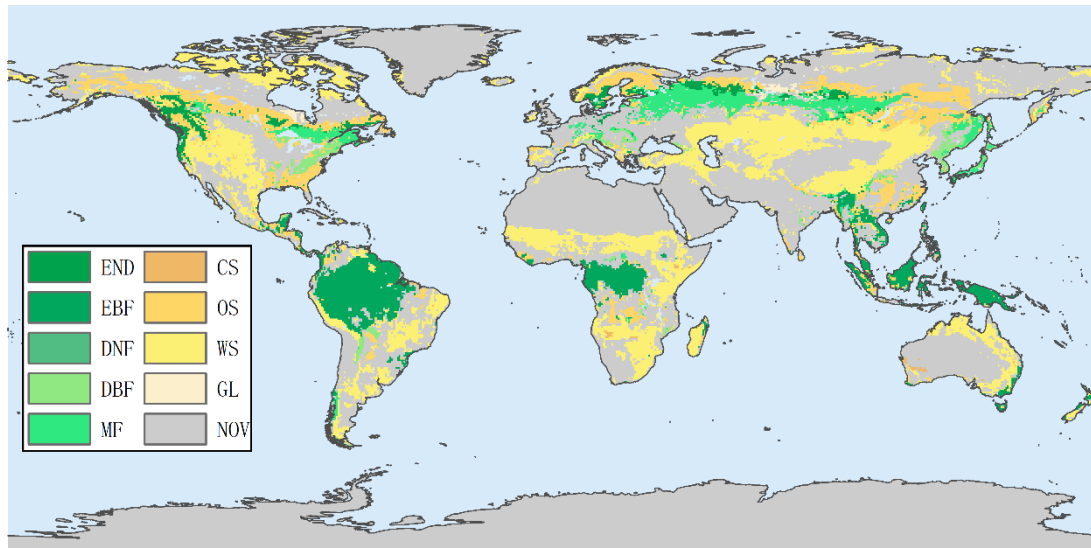


Figure A4. Spatial distribution of multi-year average fraction of managed pasture from 2001-2015 at 0.5 x 0.5 arc-degree resolution.

756



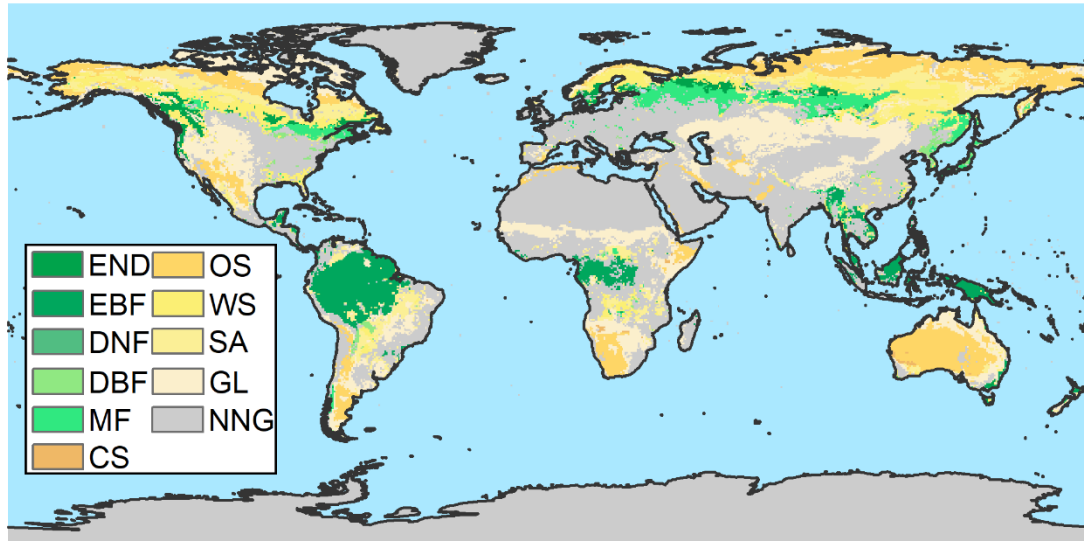


Figure [A2A5](#). [Map of land vegetation without anthropogenic disturbance from MCD12C1 and LUH2](#)~~Land vegetation cover map from MCD12C1~~. END: Evergreen needleleaf forest, EBF: Evergreen broadleaf forest, DNF: Deciduous needleleaf forest, DBF: Deciduous broadleaf forest, MF: Mixed forest, CS: Closed shrublands, OS: Open shrublands, WS: Woody savannas, [SA: Savannas](#), GL: Grasslands, [NNG: No natural vegetation, which means the zone is not covered by vegetation without anthropogenic disturbance](#)~~NOV: No value~~.

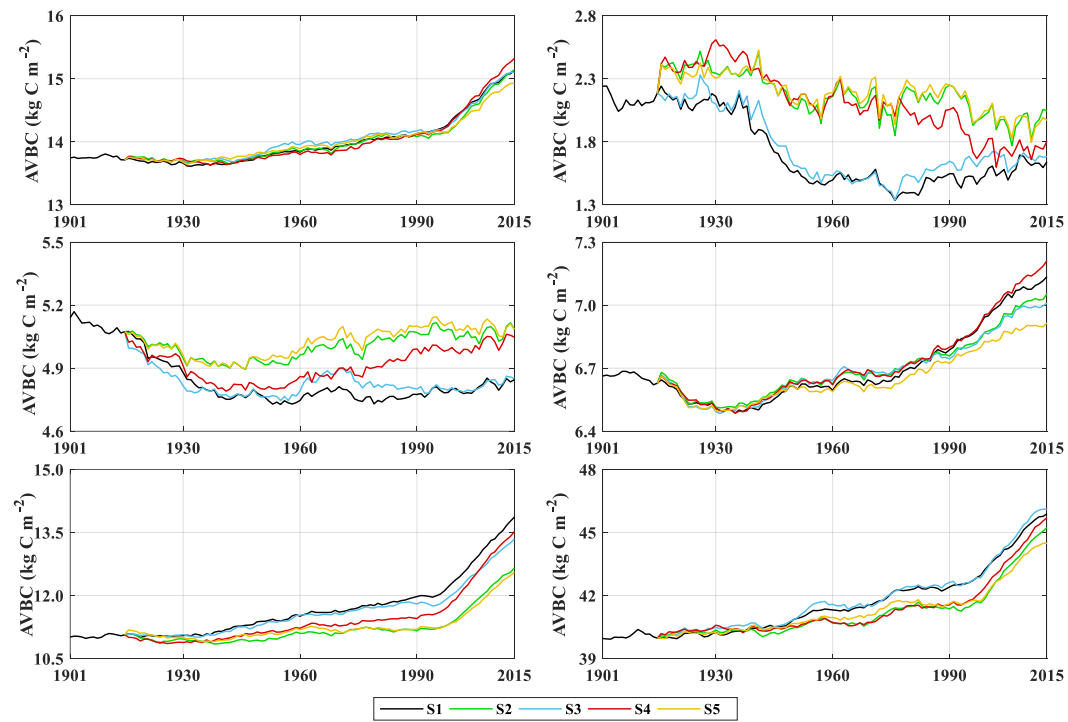
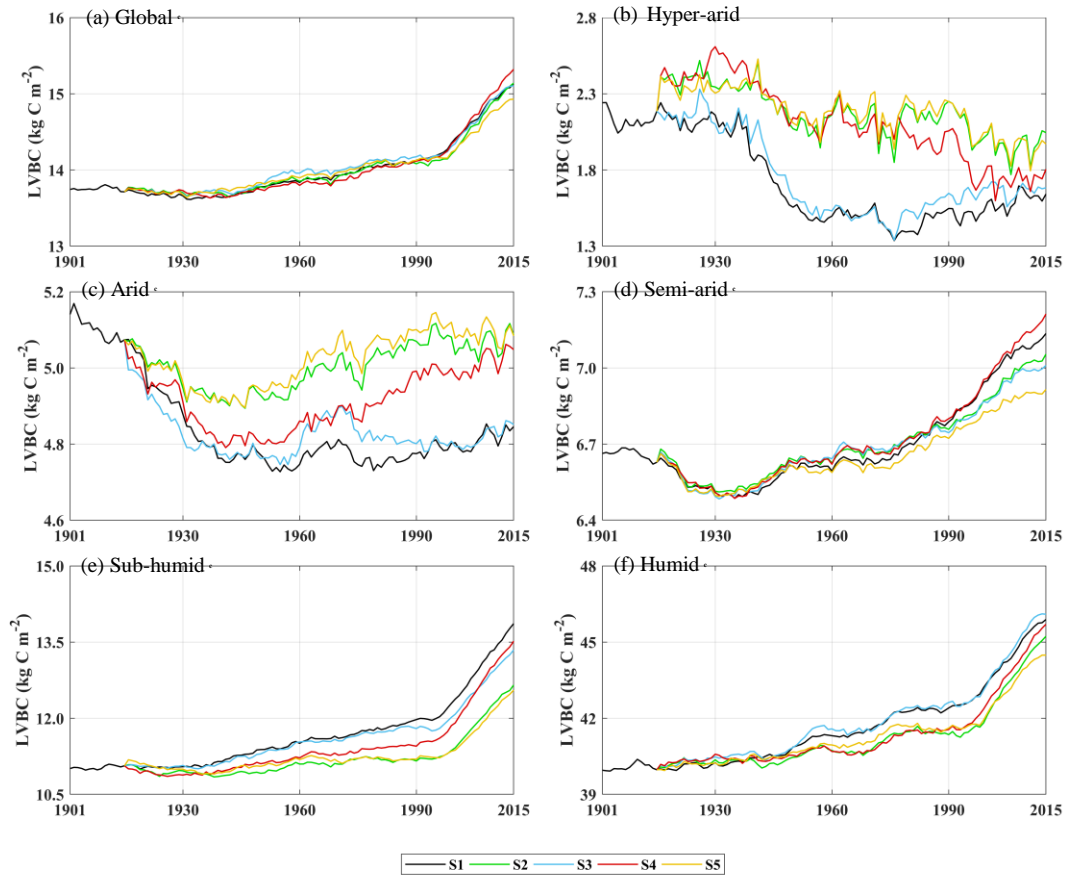
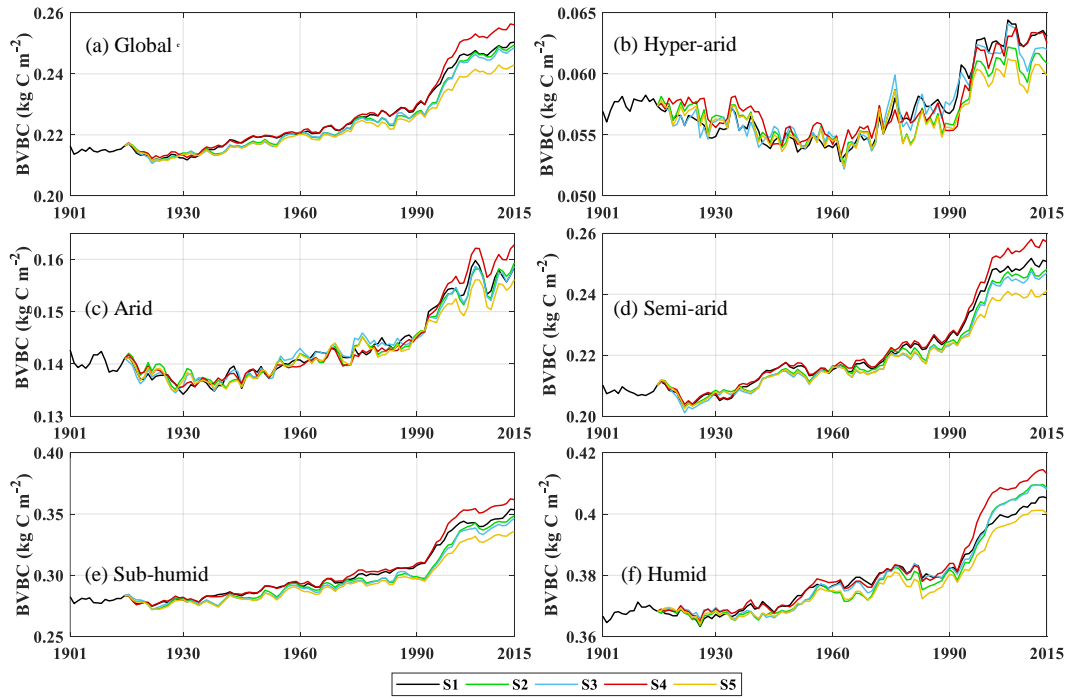


Figure A3A6. Trends in average density of potential AVBCLVBC. (a) Modelled trend of annual

averaged BVBC-LVBC globally. Modelled trends in annual averaged AVBC-LVBC in hyper-arid regionzones (b), arid regionzones (c), semi-arid regionzones (d), sub-humid regionzones (e), and humid zoneregions (f).

758



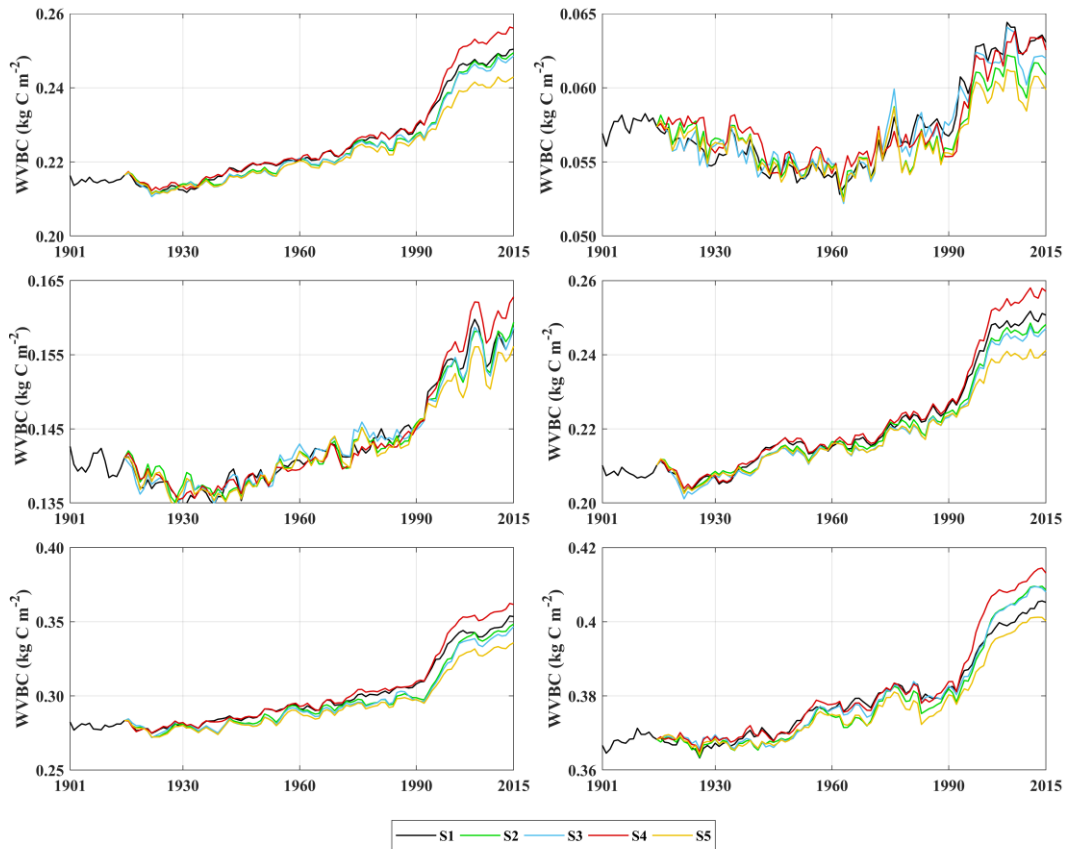


Figure A4A7. Trends in average density of potential BVBC-WVBC. (a) Modelled trend of annual averaged BVBC-WVBC globally. Modelled trends in annual averaged BVBC-WVBC in hyper-arid regionszone (b), arid regionszone (c), semi-arid regionszone (d), sub-humid regionszone (e), and humid regionszone (f).

759 **Code and data availability statement**

760 The code of SEIB-DGVM version 3.02 can be download from <http://seib-dgvm.com/>. Climatic Research  
 761 Unit data can be downloaded from <https://crudata.uea.ac.uk/cru/data/hrg/>. The soil physical parameters  
 762 can be downloaded from [www.iges.org/gswp](http://www.iges.org/gswp). The reconstructed CO<sub>2</sub> concentration dataset and SEIB  
 763 code can be downloaded from <http://seib-dgvm.com/>. In model validation, Ecosystem Model-Data  
 764 Intercomparison (multiyear average NPP product) data were collected from  
 765 [https://daac.ornl.gov/NPP/guides/NPP\\_EMDI.html](https://daac.ornl.gov/NPP/guides/NPP_EMDI.html). Remote sensing product MOD17A3 data were  
 766 obtained from <https://lpdaac.usgs.gov/products/mod17a3hgf006/>, and MCD12C1 data were obtained  
 767 from <https://ladsweb.modaps.eosdis.nasa.gov/search/order>, and LUH2 data were obtained from

768 <https://luh.umd.edu/>.

769 **Authors contributions**

770 T.S. designed research. T.S., and S.H. performed research and developed the methodology. T.S. analyzed  
771 data and produced the outputs. T.S., S.H., C.J., and X.C. wrote the first manuscript draft. W.W. and W.G.  
772 supervised the study. All the authors discussed the methodology and commented on various versions of  
773 the manuscript.

774 **Competing interests**

775 The authors declare that they have no conflict of interest.

776 **Acknowledgments**

777 This work was jointly supported by the National Natural Science Foundation of China (Grant Nos.  
778 51979071, 51779073, 91547205), the National Key Research and Development Program of China  
779 (2021YFC3201100), the Distinguished Young Fund Project of Natural Science Foundation of Jiangsu  
780 Province (BK20180021), and the National “Ten Thousand Program” Youth Talent. We thank Zefeng  
781 Chen for technical support. We gratefully thank the following data providers and model developers for  
782 their continuous efforts and for sharing their data: the University of East Anglia, the National Centers for  
783 Environmental Prediction (NCEP), the National Oceanic and Atmospheric Administration (NOAA),  
784 [University of Maryland](#), and the Center for Ocean-Land-Atmosphere Studies (COLA). [Cordial thanks](#)  
785 [are extended to the editor, Dr. Hans Verbeeck, and two anonymous referees for the valuable comments](#)  
786 [which greatly improve the quality of the paper.](#)



787 **References**

- 788 Ahlstrom, A., Raupach, M. R., Schurgers, G., Smith, B., Arneeth, A., Jung, M., Reichstein, M., Canadell,  
789 J. G., Friedlingstein, P., Jain, A. K., Kato, E., Poulter, B., Sitch, S., Stocker, B. D., Viovy, N., Wang,  
790 Y. P., Wiltshire, A., Zaehle, S., and Zeng, N.: The dominant role of semi-arid ecosystems in the  
791 trend and variability of the land CO<sub>2</sub> sink, *Science*, 348, 895-899, 10.1126/science.aaa1668, 2015.
- 792 Ajtay, G. L., Ketner, P., and Duvigneaud, P.: Terrestrial primary production and phytomass In: *The*  
793 *Global Cycle.*, Glob. Carbon Cycle, SCOPE, 129-181 pp.1979.
- 794 Anderson, L. J., Derner, J. D., Polley, H. W., Gordon, W. S., Eissenstat, D. M., and Jackson, R. B.: Root  
795 responses along a subambient to elevated CO<sub>2</sub> gradient in a C<sub>3</sub>-C<sub>4</sub> grassland, *Global Change Biol*,  
796 16, 454-468, 10.1111/j.1365-2486.2009.01975.x, 2010.
- 797 Bartholome, E. and Belward, A. S.: GLC2000: a new approach to global land cover mapping from Earth  
798 observation data, *Int J Remote Sens*, 26, 1959-1977, 10.1080/01431160412331291297, 2005.
- 799 Bayer, A. D., Pugh, T. A. M., Krause, A., and Arneeth, A.: Historical and future quantification of  
800 terrestrial carbon sequestration from a Greenhouse-Gas-Value perspective, *Global Environmental*  
801 *Change*, 32, 153-164, 10.1016/j.gloenvcha.2015.03.004, 2015.
- 802 Bazilevich, N. I., Rodin, L. Y., and Rozov, N. N.: Geographical Aspects of Biological Productivity,  
803 *Soviet Geograpy Review and Translation*, 5, 293-317 pp.1971.
- 804 Bloom, A. A., Exbrayat, J. F., van der Velde, I. R., Feng, L., and Williams, M.: The decadal state of the  
805 terrestrial carbon cycle: Global retrievals of terrestrial carbon allocation, pools, and residence times,  
806 *Proceedings of the National Academy of Sciences of the United States of America*, 113, 1285-1290,  
807 10.1073/pnas.1515160113, 2016.
- 808 Chen, J., Ju, W., Ciais, P., Viovy, N., Liu, R. G., Liu, Y., and Lu, X. H.: Vegetation structural change  
809 since 1981 significantly enhanced the terrestrial carbon sink, *Nat Commun*, 10, 4259,  
810 10.1038/S41467-019-12257-8, 2019.
- 811 Chen, L.-P., Zhao, N.-X., Zhang, L.-H., and Gao, Y.-B.: Responses of two dominant plant species to  
812 drought stress and defoliation in the Inner Mongolia Steppe of China, *Plant Ecology*, 214, 221-229,  
813 10.1007/s11258-012-0161-y, 2013.
- 814 Cheng, L., Zhang, L., Wang, Y. P., Canadell, J. G., Chiew, F. H. S., Beringer, J., Li, L. H., Miralles, D.  
815 G., Piao, S. L., and Zhang, Y. Q.: Recent increases in terrestrial carbon uptake at little cost to the  
816 water cycle, *Nat Commun*, 8, 10.1038/s41467-017-00114-5, 2017.
- 817 Erb, K.-H., Gingrich, S., Krausmann, F., and Haberl, H.: Industrialization, Fossil Fuels, and the  
818 Transformation of Land Use, *Journal of Industrial Ecology*, 12, 686-703, 10.1111/j.1530-  
819 9290.2008.00076.x, 2008.
- 820 Erb, K.-H., Gaube, V., Krausmann, F., Plutzer, C., Bondeau, A., and Haberl, H.: A comprehensive global  
821 5min resolution land-use data set for the year 2000 consistent with national census data, *Journal of*  
822 *Land Use Science*, 2, 191-224, 10.1080/17474230701622981, 2007.
- 823 Erb, K.-H., Fetzel, T., Plutzer, C., Kastner, T., Lauk, C., Mayer, A., Niedertscheider, M., Körner, C., and  
824 Haberl, H.: Biomass turnover time in terrestrial ecosystems halved by land use, *Nat Geosci*, 9, 674-  
825 678, 10.1038/ngeo2782, 2016.
- 826 Erb, K.-H., Kastner, T., Plutzer, C., Bais, A. L. S., Carvalhais, N., Fetzel, T., Gingrich, S., Haberl, H.,  
827 Lauk, C., Niedertscheider, M., Pongratz, J., Thurner, M., and Luyssaert, S.: Unexpectedly large  
828 impact of forest management and grazing on global vegetation biomass, *Nature*, 553, 73-76,  
829 10.1038/nature25138, 2018.

830 Fan, L., Wigneron, J. P., Ciais, P., Chave, J., Brandt, M., Fensholt, R., Saatchi, S. S., Bastos, A., Al-  
831 Yaari, A., Hufkens, K., Qin, Y. W., Xiao, X. M., Chen, C., Myneni, R. B., Fernandez-Moran, R.,  
832 Mialon, A., Rodriguez-Fernandez, N. J., Kerr, Y., Tian, F., and Penuelas, J.: Satellite-observed  
833 pantropical carbon dynamics, *Nat Plants*, 5, 944-951, 10.1038/s41477-019-0478-9, 2019.

834 Fang, J., Yang, Y., Ma, W., Mohammat, A., and Shen, H.: Ecosystem carbon stocks and their changes  
835 in China's grasslands, *Science China. Life sciences*, 53, 757-765, 10.1007/s11427-010-4029-x, 2010.

836 Friedlingstein, P., Joel, G., Field, C. B., and Fung, I. Y.: Toward an allocation scheme for global  
837 terrestrial carbon models, *Global Change Biol*, 5, 755-770, DOI 10.1046/j.1365-2486.1999.00269.x,  
838 1999.

839 Gentine, P., Green, J. K., Guérin, M., Humphrey, V., Seneviratne, S. I., Zhang, Y., and Zhou, S.:  
840 Coupling between the terrestrial carbon and water cycles—a review, *Environ Res Lett*, 14, 083003,  
841 10.1088/1748-9326/ab22d6, 2019.

842 Gill, R. and Jackson, R.: Global patterns of root turnover for terrestrial ecosystems, *New Phytol*, 147,  
843 13-31, [10.1046/j.1469-8137.2000.00681.x](https://doi.org/10.1046/j.1469-8137.2000.00681.x), ~~20002000~~.

844 Gocic, M. and Trajkovic, S.: Analysis of changes in meteorological variables using Mann-Kendall and  
845 Sen's slope estimator statistical tests in Serbia, *Global and Planetary Change*, 100, 172-182,  
846 10.1016/j.gloplacha.2012.10.014, 2013.

847 Gulbeyaz, O., Bond-Lamberty, B., Akyurek, Z., and West, T. O.: A new approach to evaluate the MODIS  
848 annual NPP product (MOD17A3) using forest field data from Turkey, *Int J Remote Sens*, 39, 2560-  
849 2578, 10.1080/01431161.2018.1430913, 2018.

850 Haberl, H., Erb, K. H., and Krausmann, F.: Human Appropriation of Net Primary Production: Patterns,  
851 Trends, and Planetary Boundaries, *Annu Rev Env Resour*, 39, 363-391, 10.1146/annurev-environ-  
852 121912-094620, 2014.

853 Harper, A. B., Wiltshire, A. J., Cox, P. M., Friedlingstein, P., Jones, C. D., Mercado, L. M., Sitch, S.,  
854 Williams, K., and Duran-Rojas, C.: Vegetation distribution and terrestrial carbon cycle in a carbon  
855 cycle configuration of JULES4.6 with new plant functional types, *Geosci Model Dev*, 11, 2857-  
856 2873, 10.5194/gmd-11-2857-2018, 2018.

857 Harris, I., Osborn, T. J., Jones, P., and Lister, D.: Version 4 of the CRU TS monthly high-resolution  
858 gridded multivariate climate dataset, *Scientific Data*, 7, 109, 10.1038/s41597-020-0453-3, 2020.

859 Hovenden, M. J., Newton, P. C., and Wills, K. E.: Seasonal not annual rainfall determines grassland  
860 biomass response to carbon dioxide, *Nature*, 511, 583-586, 10.1038/nature13281, 2014.

861 Humphrey, V., Zscheischler, J., Ciais, P., Gudmundsson, L., Sitch, S., and Seneviratne, S. I.: Sensitivity  
862 of atmospheric CO<sub>2</sub> growth rate to observed changes in terrestrial water storage, *Nature*, 560, 628-  
863 631, 10.1038/s41586-018-0424-4, 2018.

864 Humphrey, V., Berg, A., Ciais, P., Gentine, P., Jung, M., Reichstein, M., Seneviratne, S. I., and  
865 Frankenberg, C.: Soil moisture–atmosphere feedback dominates land carbon uptake variability,  
866 *Nature*, 592, 65-69, 10.1038/s41586-021-03325-5, 2021.

867 Hurtt, G. C., Chini, L. P., Frolking, S., Betts, R. A., Feddema, J., Fischer, G., Fisk, J. P., Hibbard, K.,  
868 Houghton, R. A., Janetos, A., Jones, C. D., Kindermann, G., Kinoshita, T., Goldewijk, K. K., Riahi,  
869 K., Shevliakova, E., Smith, S., Stehfest, E., Thomson, A., Thornton, P., van Vuuren, D. P., and  
870 Wang, Y. P.: Harmonization of land-use scenarios for the period 1500-2100: 600 years of global  
871 gridded annual land-use transitions, wood harvest, and resulting secondary lands, *Climate Change*,  
872 109, 117-161, 10.1007/s10584-011-0153-2, 2011.

873 Hurtt, G. C., Chini, L., Sahajpal, R., Frolking, S., Bodirsky, B. L., Calvin, K., Doelman, J. C., Fisk, J.,

874 [Fujimori, S., Goldewijk, K. K., Hasegawa, T., Havlik, P., Heinemann, A., Humpenöder, F.,](#)  
875 [Jungclaus, J., Jed Kaplan, Kennedy, J., Kristzin, T., Lawrence, D., Lawrence, P., Ma, L., Mertz, O.,](#)  
876 [Pongratz, J., Popp, A., Poulter, B., Riahi, K., Shevliakova, E., Stehfest, E., Thornton, P., Tubiello,](#)  
877 [F. N., van Vuuren, D. P., Zhang, X.: Harmonization of Global Land-Use Change and Management](#)  
878 [for the Period 850-2100 \(LUH2\) for CMIP6, Geoscientific Model Development, 13, 5425-5464,](#)  
879 [10.5194/gmd-13-5425-2020, 2021.](#)

880 IPCC: Impacts, Adaptation and Vulnerability. Contribution of Working Group II to the Fourth  
881 Assessment Report of the Intergovernmental Panel on Climate Change, 2007.

882 Jung, M., Reichstein, M., Schwalm, C. R., Huntingford, C., Sitch, S., Ahlstrom, A., Arneeth, A., Camps-  
883 Valls, G., Ciais, P., Friedlingstein, P., Gans, F., Ichii, K., Jain, A. K., Kato, E., Papale, D., Poulter,  
884 B., Raduly, B., Rodenbeck, C., Tramontana, G., Viovy, N., Wang, Y. P., Weber, U., Zaehle, S., and  
885 Zeng, N.: Compensatory water effects link yearly global land CO<sub>2</sub> sink changes to temperature,  
886 Nature, 541, 516-520, 10.1038/nature20780, 2017.

887 Kaplan, J. O., Krumhardt, K. M., Ellis, E. C., Ruddiman, W. F., Lemmen, C., and Goldewijk, K. K.:  
888 Holocene carbon emissions as a result of anthropogenic land cover change, Holocene, 21, 775-791,  
889 10.1177/0959683610386983, 2011.

890 Keenan, T. F., Prentice, I. C., Canadell, J. G., Williams, C. A., Wang, H., Raupach, M., and Collatz, G.  
891 J.: Recent pause in the growth rate of atmospheric CO<sub>2</sub> due to enhanced terrestrial carbon uptake  
892 Nat Commun, 7, 10.1038/Ncomms16137, 2017.

893 Kindermann, G. E., Mcallum, I., Fritz, S., and Obersteiner, M.: A global forest growing stock, biomass  
894 and carbon map based on FAO statistics, Silva Fenn, 42, 387-396, 10.14214/Sf.244, 2008.

895 Le Noë, J., Matej, S., Magerl, A., Bhan, M., Erb, K. H., and Gingrich, S.: Modeling and empirical  
896 validation of long-term carbon sequestration in forests (France, 1850-2015), Glob Chang Biol, 26,  
897 2421-2434, 10.1111/gcb.15004, 2020.

898 Liu, J., Bowman, K. W., Schimel, D. S., Parazoo, N. C., Jiang, Z., Lee, M., Bloom, A. A., Wunch, D.,  
899 Frankenberg, C., Sun, Y., O'Dell, C. W., Gurney, K. R., Menemenlis, D., Gierach, M., Crisp, D.,  
900 and Eldering, A.: Contrasting carbon cycle responses of the tropical continents to the 2015-2016 El  
901 Nino, Science, 358, eaam5690, 10.1126/science.aam5690, 2017.

902 Ma, H. Z., Mo, L. D., Crowther, T. W., Maynard, D. S., van den Hoogen, J., Stocker, B. D., Terrer, C.,  
903 and Zohner, C. M.: The global distribution and environmental drivers of aboveground versus  
904 belowground plant biomass, Nat Ecol Evol, 5, 1110+, 10.1038/s41559-021-01485-1, 2021.

905 Madani, N., Parazoo, N. C., Kimball, J. S., Ballantyne, A. P., Reichle, R. H., Maneta, M., Saatchi, S.,  
906 Palmer, P. I., Liu, Z., and Tagesson, T.: Recent Amplified Global Gross Primary Productivity Due  
907 to Temperature Increase Is Offset by Reduced Productivity Due to Water Constraints, AGU  
908 Advances, 2, e2020AV000180, 10.1029/2020AV000180, 2020.

909 Magerl, A., Le Noë, J., Erb, K.-H., Bhan, M., and Gingrich, S.: A comprehensive data-based assessment  
910 of forest ecosystem carbon stocks in the U.S. 1907–2012, Environ Res Lett, 14, 125015,  
911 10.1088/1748-9326/ab5cb6, 2019.

912 McConnaughay, K. D. M. and Coleman, J. S.: Biomass allocation in plants: ontogeny or optimality? A  
913 test along three resource gradients, Ecology, 80, 2581-2593, 10.1890/0012-  
914 9658(1999)080[2581:BAIPOO]2.0.CO;2, 1999.

915 Monteith, J. L. and Unsworth, M. H.: Principles of Environmental Physics, 2nd ed., London1990.

916 Olson, J., Watts, J., and Allison, L.: Carbon in Live Vegetation of Major World Ecosystems, Oak Ridge  
917 National Laboratory1983.

918 Pan, Y. D., Birdsey, R. A., Phillips, O. L., and Jackson, R. B.: The Structure, Distribution, and Biomass  
919 of the World's Forests, *Annu Rev Ecol Evol S*, 44, 593-622, 10.1146/annurev-ecolsys-110512-  
920 135914, 2013.

921 Pan, Y. D., Birdsey, R. A., Fang, J. Y., Houghton, R., Kauppi, P. E., Kurz, W. A., Phillips, O. L.,  
922 Shvidenko, A., Lewis, S. L., Canadell, J. G., Ciais, P., Jackson, R. B., Pacala, S. W., McGuire, A.  
923 D., Piao, S. L., Rautiainen, A., Sitch, S., and Hayes, D.: A Large and Persistent Carbon Sink in the  
924 World's Forests, *Science*, 333, 988-993, 10.1126/science.1201609, 2011.

925 Piao, S. L., Friedlingstein, P., Ciais, P., Zhou, L. M., and Chen, A. P.: Effect of climate and CO2 changes  
926 on the greening of the Northern Hemisphere over the past two decades, *Geophys Res Lett*, 33,  
927 L23402, 10.1029/2006GL028205, 2006.

928 Piao, S. L., Wang, X., Wang, K., Li, X., Bastos, A., Canadell, J. G., Ciais, P., Friedlingstein, P., and  
929 Sitch, S.: Interannual variation of terrestrial carbon cycle: Issues and perspectives, *Glob Chang Biol*,  
930 26, 300-318, 10.1111/gcb.14884, 2020.

931 Poorter, H.: Construction costs and payback time of biomass: a whole plant perspective, *A Whole-Plant  
932 Perspective on Carbon-Nitrogen Interactions*, SPB Academic Publishing, The Hague 1994.

933 Poulter, B., Frank, D., Ciais, P., Myneni, R. B., Andela, N., Bi, J., Broquet, G., Canadell, J. G., Chevallier,  
934 F., Liu, Y. Y., Running, S. W., Sitch, S., and van der Werf, G. R.: Contribution of semi-arid  
935 ecosystems to interannual variability of the global carbon cycle, *Nature*, 509, 600-603,  
936 10.1038/nature13376, 2014.

937 Prentice, I. C., Harrison, S. P., and Bartlein, P. J.: Global vegetation and terrestrial carbon cycle changes  
938 after the last ice age, *New Phytol*, 189, 988-998, 10.1111/j.1469-8137.2010.03620.x, 2011.

939 Roy, J., Saugier, B., and Mooney, H. A.: Estimations of global terrestrial productivity: converging toward  
940 a single number? In: *Terrestrial Global Productivity*, Academic Press, San Diego 2001.

941 Ruesch, A. and Gibbs, H. K.: New IPCC Tier-1 global biomass carbon map for the year 2000, 2008.

942 Ryan, M. G.: Effects of Climate Change on Plant Respiration, *Ecological Applications*, 1, 157-167,  
943 10.2307/1941808, 1991.

944 Sato, H., Itoh, A., and Kohyama, T.: SEIB-DGVM: A new Dynamic Global Vegetation Model using a  
945 spatially explicit individual-based approach, *Ecological Modelling*, 200, 279-307,  
946 10.1016/j.ecolmodel.2006.09.006, 2007.

947 Sato, H., Kobayashi, H., Beer, C., and Fedorov, A.: Simulating interactions between topography,  
948 permafrost, and vegetation in Siberian larch forest, *Environ Res Lett*, 15, 095006, 10.1088/1748-  
949 9326/Ab9be4, 2020.

950 Saugier, B., Roy, J., and Mooney, H.: Estimations of Global Terrestrial Productivity, *Terrestrial Global  
951 Productivity*, Academic Press, San Diego, Calif 2001.

952 Schimel, D., Stephens, B. B., and Fisher, J. B.: Effect of increasing CO2 on the terrestrial carbon cycle,  
953 *Proceedings of the National Academy of Sciences of the United States of America*, 112, 436-441,  
954 10.1073/pnas.1407302112, 2015.

955 Seo, H. and Kim, Y.: Interactive impacts of fire and vegetation dynamics on global carbon and water  
956 budget using Community Land Model version 4.5, *Geosci Model Dev*, 12, 457-472, 10.5194/gmd-  
957 12-457-2019, 2019.

958 Shevliakova, E., Pacala, S. W., Malyshev, S., Hurtt, G. C., Milly, P. C. D., Caspersen, J. P., Sentman, L.  
959 T., Fisk, J. P., Wirth, C., and Crevoisier, C.: Carbon cycling under 300 years of land use change:  
960 Importance of the secondary vegetation sink, *Global Biogeochem Cy*, 23, 10.1029/2007gb003176,  
961 2009.

962 Sun, F., Roderick, M. L., and Farquhar, G. D.: Changes in the variability of global land precipitation,  
963 *Geophys Res Lett*, 39, L19402, 10.1029/2012gl053369, 2012.

964 Tei, S., Sugimoto, A., Liang, M. C., Yonenobu, H., Matsuura, Y., Osawa, A., Sato, H., Fujinuma, J., and  
965 Maximov, T.: Radial Growth and Physiological Response of Coniferous Trees to Arctic  
966 Amplification, *J Geophys Res-Bioge*, 122, 2786-2803, 10.1002/2016JG003745, 2017.

967 Terrer, C., Phillips, R. P., Hungate, B. A., Rosende, J., Pett-Ridge, J., Craig, M. E., van Groenigen, K. J.,  
968 Keenan, T. F., Sulman, B. N., Stocker, B. D., Reich, P. B., Pellegrini, A. F. A., Pendall, E., Zhang,  
969 H., Evans, R. D., Carrillo, Y., Fisher, J. B., Van Sundert, K., Vicca, S., and Jackson, R. B.: A trade-  
970 off between plant and soil carbon storage under elevated CO<sub>2</sub>, *Nature*, 591, 599-603,  
971 10.1038/s41586-021-03306-8, 2021.

972 Tharammal, T., Bala, G., Devaraju, N., and Nemani, R.: A review of the major drivers of the terrestrial  
973 carbon uptake: model-based assessments, consensus, and uncertainties, *Environ Res Lett*, 14,  
974 093005, 10.1088/1748-9326/Ab3012, 2019.

975 Tong, X. W., Brandt, M., Yue, Y. M., Ciais, P., Jepsen, M. R., Penuelas, J., Wigner, J. P., Xiao, X.  
976 M., Song, X. P., Horion, S., Rasmussen, K., Saatchi, S., Fan, L., Wang, K. L., Zhang, B., Chen, Z.  
977 C., Wang, Y. H., Li, X. J., and Fensholt, R.: Forest management in southern China generates short  
978 term extensive carbon sequestration, *Nat Commun*, 11, 10.1038/s41467-019-13798-8, 2020.

979 West, P. C., Gibbs, H. K., Monfreda, C., Wagner, J., Barford, C. C., Carpenter, S. R., and Foley, J. A.:  
980 Trading carbon for food: Global comparison of carbon stocks vs. crop yields on agricultural land,  
981 *Proceedings of the National Academy of Sciences of the United States of America*, 107, 19645-  
982 19648, 10.1073/pnas.1011078107, 2010.

983 Wild, M., Gilgen, H., Roesch, A., Ohmura, A., Long, C. N., Dutton, E. G., Forgan, B., Kallis, A., Russak,  
984 V., and Tsvetkov, A.: From dimming to brightening: Decadal changes in solar radiation at Earth's  
985 surface, *Science*, 308, 847-850, 10.1126/science.1103215, 2005.

986 Yang, Y., Fang, J., Ma, W., Guo, D., and Mohammat, A.: Large-scale pattern of biomass partitioning  
987 across China's grasslands, *Global Ecology and Biogeography*, 19, 268-277, 10.1111/j.1466-  
988 8238.2009.00502.x, 2010.

989 Zhang, H., Song, T. Q., Wang, K. L., Yang, H., Yue, Y. M., Zeng, Z. X., Peng, W. X., and Zeng, F. P.:  
990 Influences of stand characteristics and environmental factors on forest biomass and root-shoot  
991 allocation in southwest China, *Ecol Eng*, 91, 7-15, 10.1016/j.ecoleng.2016.01.040, 2016.

992 Zhu, Z. C., Piao, S. L., Myneni, R. B., Huang, M. T., Zeng, Z. Z., Canadell, J. G., Ciais, P., Sitch, S.,  
993 Friedlingstein, P., Arneeth, A., Cao, C. X., Cheng, L., Kato, E., Koven, C., Li, Y., Lian, X., Liu, Y.  
994 W., Liu, R. G., Mao, J. F., Pan, Y. Z., Peng, S. S., Penuelas, J., Poulter, B., Pugh, T. A. M., Stocker,  
995 B. D., Viovy, N., Wang, X. H., Wang, Y. P., Xiao, Z. Q., Yang, H., Zaehle, S., and Zeng, N.:  
996 Greening of the Earth and its drivers, *Nat Clim Change*, 6, 791-+, 10.1038/Nclimate3004, 2016.